The KH domains of FMRP differentially regulate neuronal granule formation, dynamics, and function in *Drosophila*

Emily L. Starke[1] and Scott A. Barbee[1,2,*]

[1]Department of Biological Sciences, University of Denver, Denver, Colorado, 80210, USA [2]Molecular and Cellular Biophysics Program, University of Denver, Denver, Colorado, 80210, USA

*Correspondence: scott.barbee@du.edu

ABSTRACT

Fragile X Syndrome (FXS) is the most prevalent cause of inherited mental deficiency and is the most common monogenetic cause of autism spectral disorder (ASD). Here, we demonstrate that disease-causing missense mutations in the conserved K homology (KH) RNA binding domains (RBDs) of FMRP cause defects in its ability to form RNA transport granules in neurons. Using molecular, genetic, and imaging approaches in the *Drosophila* FXS model system, we show that the KH1 and KH2 domains of FMRP regulate distinct aspects of neuronal FMRP granule formation, dynamics, and transport. Furthermore, mutations in both KH domains disrupt translational repression in cells and the localization of known FMRP target mRNAs in neurons. These results suggest that the KH domains play an essential role in neuronal FMRP granule formation and function which may be linked to the molecular pathogenesis of FXS.

KEYWORDS

Drosophila, Fragile X Syndrome, FMRP, KH domain, RNA granules, RNA localization, translational regulation, phase separation

46 **INTRODUCTION**

47 Fragile X Syndrome (FXS) is the most common cause of inherited intellectual
48 disability in humans (Santoro et al., 2012). Typically, FXS is caused by epigenetic
49 silencing of the *FMR1* gene due to a long CGG repeat expansion in the 5'UTR, resulting
50 in hypermethylation of the *FMR1* locus and subsequent transcriptional silencing (Pieretti
51 et al., 1991). This results in loss of expression of the encoded Fragile X Mental
52 Retardation Protein (FMRP), an evolutionarily conserved RNA-binding protein (RBP) that
53 binds to many mRNAs in the mammalian brain. FMRP is best characterized as a
54 translational repressor (Richter and Zhao, 2021). In this role, FMRP associates with
55 diverse ribonucleoprotein particles (RNPs) including RNA transport granules, P-bodies
56 (PBs), and stress granules (SGs) (Lai et al., 2020). In neurons, FMRP-containing RNA
57 transport granules (hereafter called "FMRP granules") are actively transported in both
58 axons and dendrites (Antar et al., 2005; Antar et al., 2006; Dictenberg et al., 2008; Li et
59 al., 2009). These granules carry translationally repressed mRNAs to synapses where they
60 are derepressed in response to synaptic activity. Local translation of critical mRNAs at
61 synapses is essential for long-term synaptic plasticity and is defective in FXS.

62 The role of FMRP in translation and mRNA transport in the context of neurons
63 remains enigmatic. In the soma, FMRP binds to translationally repressed target mRNAs
64 and associated RBPs. These RNPs merge and are remodeled to allow for rapid, motor-
65 dependent transport within neurites (El Fatimy et al., 2016). FMRP granules belong to a
66 diverse class of membraneless organelles (MLOs) that form through liquid-liquid phase
67 separation (LLSP) (Banani et al., 2017). This process is driven by weak, multivalent
68 interactions between protein and RNA components (Mittag and Parker, 2018; Van Treeck

69 and Parker, 2018). Weak interactions allow MLOs to be highly dynamic and to rapidly
70 assemble and disassemble in response to local signals. In the case of FMRP,
71 posttranslational modification of its C-terminal intrinsically disordered region (IDR) can
72 reversibly control its phase separation *in vitro,* a process that correlates with translational
73 repression (Tsang et al., 2019). This is an attractive model to explain how FMRP granules
74 might assemble, deliver translationally repressed mRNAs to the synapse, and then
75 regulate their local translation in response to activity. However, it is unclear whether the
76 IDR acts alone or together with structured RBDs to regulate FMRP granules *in vivo*.

77 Although the most common cause of FXS is loss-of-function, advances in gene
78 sequencing have led to the discovery of FXS-causing missense mutations in the *FMR1*
79 gene (Suhl and Warren, 2015). Two mutations located in structured N-terminal RBDs of
80 FMRP and have been functionally characterized (De Boulle et al., 1993; Feng et al., 1997;
81 Myrick et al., 2015a; Myrick et al., 2015b; Prieto et al., 2021; Zang et al., 2009). The
82 Gly266Glu (G266E) and Ile304Asn (I304N) mutations are in K-homology domains (KH1
83 and KH2 respectively) which bind to “kissing-complex” tertiary motifs or distinct sequence
84 elements (GACR, ACUK, and WGGA) within target mRNAs (Ascano et al., 2012; Darnell
85 et al., 2005; Ray et al., 2013). The latter are ubiquitous sequences in mammalian
86 transcripts (Suhl et al., 2014). The analysis of these mutations has begun to uncover
87 novel functions for *FMR1*. For example, both the G266E and I304N disrupt the ability of
88 FMRP to bind to specific target mRNAs and to associate with polysomes suggesting that
89 the KH domains are important for translational regulation (Myrick et al., 2014; Zang *et al.*,
90 2009). However, the precise role these domains play in FMRP granule formation,
91 dynamics, and function in the context of neurons remains unknown.

92 Studying FMRP function in mammals is genetically complicated due to the
93 presence of two autosomal paralogs, FXR1P and FXR2P, which have some functional
94 redundancy with FMRP (Agulhon et al., 1999; Wan et al., 2000; Zhang et al., 1995). In
95 contrast, *Drosophila* has a single *dFmr1* gene and the dFMRP protein shares significant
96 sequence identity with mammalian FMRP, particularly within the RBDs (Wan *et al.*, 2000).
97 *Drosophila* FMRP granules are also compositionally like those observed in mammalian
98 neurons(Barbee et al., 2006; Cougot et al., 2008). Importantly, *Drosophila* has proven to
99 be an excellent model system in which to study FXS because *dFmr1* mutants recapitulate
100 many FXS phenotypes (Drozd et al., 2018). Here, we have introduced analogous
101 mutations into the KH1 and KH2 domains of dFMRP (G269E and I307N respectively) and
102 examined FMRP granules in *Drosophila* Schneider (S2) cells and primary neurons.
103 Analysis of these mutants has revealed distinct differences in the requirement for KH1
104 and KH2 in the formation and dynamics of FMRP granules. Interestingly, both FXS-
105 causing KH mutations result in FMRP granules that are significantly more dynamic. This
106 is in opposition to mutations in other RBPs that drive the formation of solid-like aggregates
107 associated with neurodegenerative disorders. Finally, the KH mutations differentially
108 impact the function of FMRP in translational repression and RNA transport. Our findings
109 provide new biological insight into the normal function of FMRP in cells and neurons and
110 into the specific molecular and cellular processes that are dysregulated in FXS.
111

112 **RESULTS**

113 **The KH domains are required to form FMRP granules in cells**

114 The C-terminal IDR of mammalian FMRP is necessary and sufficient to drive the
115 formation of phase-separated liquid droplets *in vitro* (Tsang *et al.*, 2019). However, the
116 dependency of the IDR in FMRP granule formation in cells has yet to be elucidated. To
117 address this, we first developed dFMRP deletion and mutant transgenes (Figure 1A).
118 Unless otherwise noted, EGFP was fused to the N-terminus to visualize granules.
119 Overexpression of GFP-tagged wild-type dFMRP (WT-FMRP) in *Drosophila* larval motor
120 neurons (MNs) replicated published results with untagged dFMRP indicating that GFP
121 does not significantly interfere with protein function (Figure S1) (Zhang et al., 2001).

122 The C-terminus of dFMRP is predicted to be disordered, indicating it may play an
123 important role in promoting LLPS (Figure 1A). We first transfected *Drosophila* S2R+ cells
124 with WT-dFMRP, $dFMRP_{\Delta IDR}$ (ΔIDR), and $dFMRP_{IDR}$ (IDR) (Figure 1B-C). As shown
125 previously, 98% of cells transfected with WT-FMRP form numerous small round granules
126 (Figure 1C-D) (Gareau et al., 2013a; Gareau et al., 2013b). We found that the IDR alone
127 was sufficient to induce FMRP granules in 65% of transfected cells (Figure 1C-D). These
128 granules were morphologically like WT-FMRP albeit less numerous (Figure 1E-F).
129 Interestingly, the structured N-terminal domain of dFMRP (ΔIDR) was also sufficient to
130 induce granule formation in 26% of cells (Figure 1C-D). These granules were less
131 abundant, and many had an amorphic (non-circular) morphology (Figure 1E-F). This
132 suggests that, unlike human FMRP *in vitro*, the C-terminal IDR of dFMRP is not essential
133 for FMRP granule formation in cells (Tsang *et al.*, 2019).

134 We speculated that the N-terminal KH1 and KH2 domains may act cooperatively
135 with the IDR to regulate FMRP granule formation. Fusing the KH domains to the IDR
136 (KH+IDR) significantly increased the number of cells containing granules (Figure 1D).

Figure 1. The KH domains and IDR interact to regulate FMRP granule formation

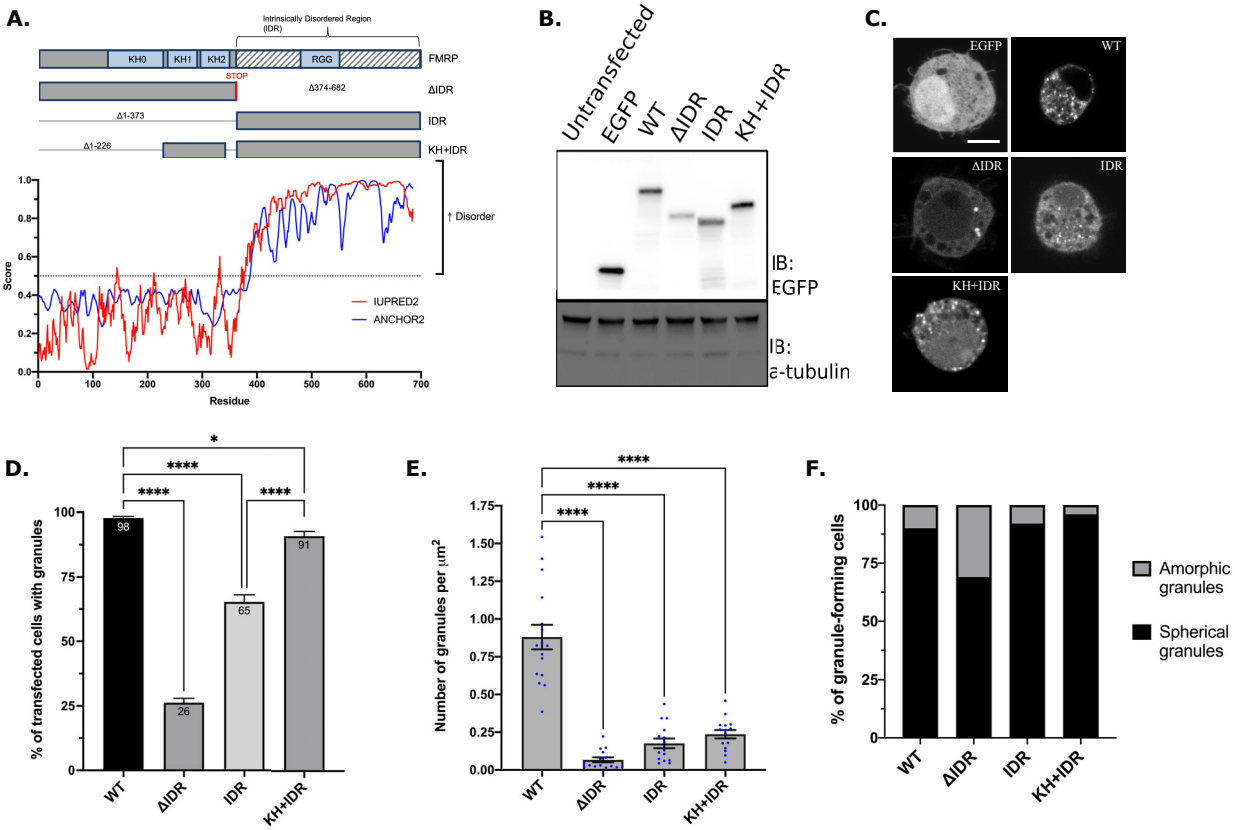

Figure 1: The KH domains and IDR interact to regulate FMRP granule formation
(A) Schematic of dFMRP showing each of the main RBDs in light blue boxes and IDR indicated by grey and white stripes (top). IDR mutants denote amino acid deletions with lines. Both KH1 and KH2 domains are fused to the IDR in the KH+IDR mutant. Disorder plot aligned with the wild-type dFMRP protein show that the C-terminus is entirely disordered as predicted by IUPRED2 and ANCHOR2 [72]. (B) Western blot analysis of EGFP (GFP) and α-tubulin (loading control) protein levels in transfected cells. (C) Representative images of GFP-FMRP mutant granule phenotypes in transfected S2R+ cells. Scale bar = 2μm. (D) Percentage of transfected cells forming GFP-FMRP granules. Data are presented as mean ± S.E. of three independent experiments (approximately 100 cells per experiment; one-way ANOVA). (E) Quantification of the number of granules counted within a cell, which was normalized to cell area in μm^2 (mean ± SE; n=15 cells; Brown-Forsyth test). (F) Quantification of the two major morphological phenotypes observed in IDR mutants (n=100 cells). In D and E, * $p<0.05$; **** $p<0.0001$.

137 These foci were morphologically indistinct from WT-FMRP granules although the number
138 of KH+IDR granules per cell did not increase significantly (Figure 1C and 1E-F). These
139 data indicate that the propensity to form granules is enhanced by addition of the KH
140 domains to the IDR. However, our results also suggest that additional elements in the N-
141 terminus are likely to be involved in the control of FMRP granule formation.
142

143 **FXS-causing mutations in the KH domains disrupt granule formation**

144 We next wanted to explore the contribution of the KH domains in FMRP granule
145 formation. The G266E and I304N missense mutations in KH1 and KH2 of hsFMRP are
146 predicted to disrupt the proper folding of each RBD and to disrupt functions of FMRP
147 including mRNA-binding, AMPA receptor trafficking, and polysome association (Darnell
148 *et al.*, 2005; Myrick *et al.*, 2014; Valverde et al., 2007). To address this, we made
149 analogous point mutations in the KH domains of dFMRP (G269E and I307N), hereafter
150 referred to as KH1* and KH2* (Figure 2A). In contrast to WT-FMRP, overexpression of
151 the GFP-tagged KH1* and KH2* transgenes in larval MNs did not inhibit axon terminal
152 growth at the neuromuscular junction (NMJ) (Figure S1) (Zhang *et al.*, 2001).

153 We transfected S2R+ cells with GFP-tagged constructs to determine the impact
154 these mutations had on FMRP granule formation. Interestingly, we observed a > 2-fold
155 decrease in the ability of cells expressing GFP-tagged KH1* to form granules relative to
156 WT-FMRP, while KH2* had no effect (Figure 2C-D). This decrease cannot be explained
157 by a difference in the expression levels of GFP-KH1* (Figure 2B). We also found that the
158 number of granules per cell was significantly reduced by both mutations, although,
159 granules were about twice as abundant in KH2* than KH1* (Figure 2E). Many KH2*

Figure 2: The KH domains are differentially required to regulate FMRP granule formation

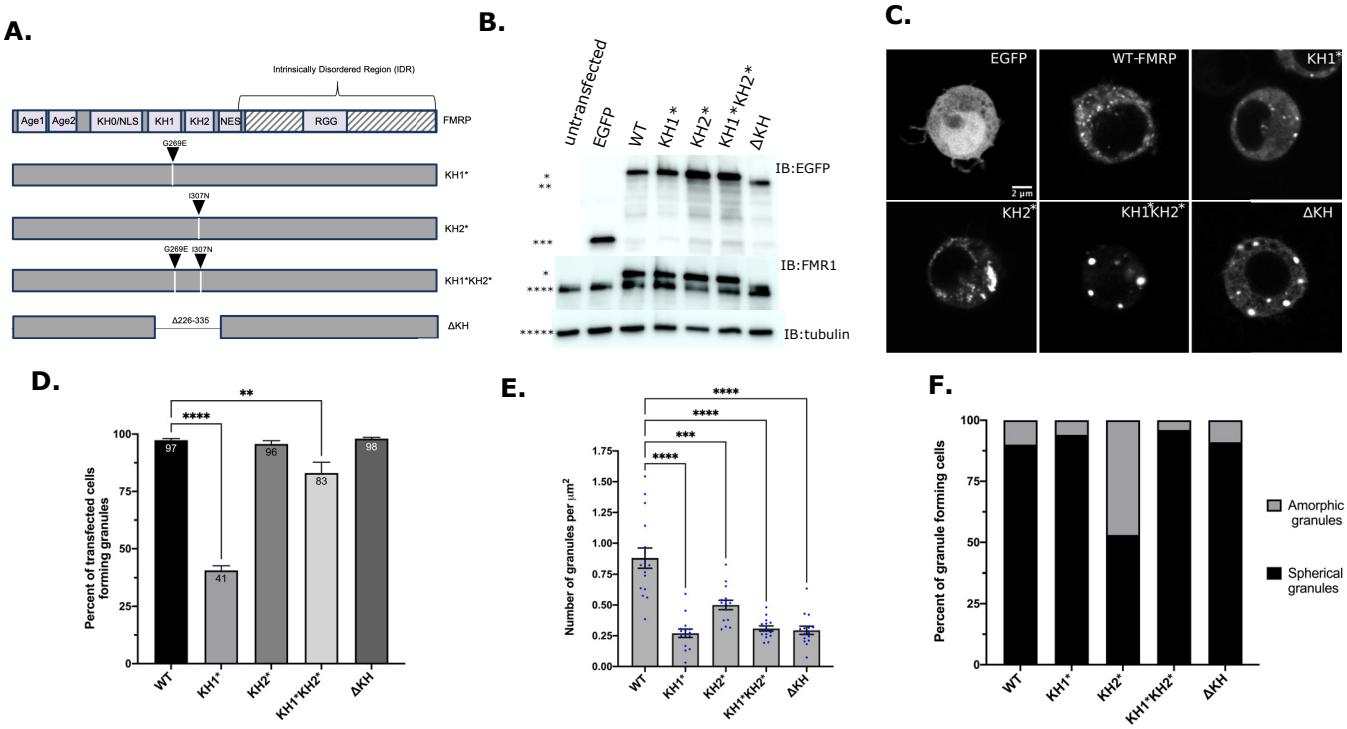

Figure 2: The KH domains differentially regulate FMRP granule formation
(A) Schematic representation of dFMRP variants used in this study. Arrowheads indicate where analogous FXS-causing point mutations were made in dFMRP. Deletion of the KH1 and KH2 domains is annotated with a break in FMRP sequence. (B) Western blot analysis of EGFP (GFP), FMRP, and α-tubulin protein levels in transfected cells. α-tubulin was used as a loading control (*= 100 kDa, **= 90 kDa, ***= 30 kDa, ****= 80 kDa, *****= 60 kDa). (C) Representative images of cells transiently transfected with the indicated GFP-tagged FMRP constructs. Scale bar = 2 µm. (D) Percentage of transfected cells forming GFP-FMRP granules. Data are presented as mean ± S.E. (approximately 100 cells per three experiments; one-way ANOVA). (E) Quantification of the number of granules per cell, which was normalized to cell area in μm^2 (mean ± SE; n=15 cells each; Brown-Forsyth test). (F) Quantification of the two major morphological phenotypes observed (n=100 cells each). In D and E, **p<0.01, ***p<0.001, ****p<0.0001.

160 granules also had an unusual, often large, amorphic structure while both WT-FMRP and
161 KH1* granules were generally small and round (Figure 2C and 2F). These results suggest
162 that both the KH1 and KH2 mutants alter normal FMRP granule formation. They also
163 suggest that each KH domain control a different aspect of this process.

164 To examine the collective contribution of both domains, we made a G269E/I307N
165 double mutant (KH1*KH2*) (Figure 2A). Most cells transfected with these constructs were
166 able to form granules (Figure 2C-D). As with the individual KH mutants, transfected cells
167 contained fewer granules per cell (Figure 2E). Interestingly, most KH1*KH2* granules that
168 formed in cells were large and round indicating that they are different from those
169 containing WT-FMRP, KH1*, or KH2* (Figure 2C and 2F). Morphologically these were
170 like a published mutant where both KH domains have been deleted (ΔKH) (Gareau *et al.*,
171 2013a; Gareau *et al.*, 2013b). Together, these data suggest that the KH domains work
172 together to restrict the size and shape of FMRP granules. However, we cannot rule out
173 that the disruption of both KH domains is changing overall protein structure which is
174 causing the formation of aggregates containing GFP-ΔKH and GFP-KH1*KH2* protein.
175

176 **FXS-causing mutations in the KH domains alter the dynamics of FMRP granules**

177 A defining feature of phase separated RNPs in cells is the ability of components to
178 rapidly shuttle between granules and the cytosol. The driving force underlying this
179 process is multivalent interactions between protein and RNA components (Shin and
180 Brangwynne, 2017). To examine whether the G269E and I307N mutations influenced
181 dFMRP dynamics, we first conducted Fluorescence Recovery After Photobleaching
182 (FRAP) experiments in S2R+ cells. The fluorescent signal of GFP-tagged WT-FMRP

183 recovered to 82% with a $t_{1/2}$ of 21.9s, in agreement with published results (Figure 3C-D)
184 (Gareau *et al.*, 2013b). We found that the exchangeable pool of KH1* and KH2* was like
185 WT-FMRP (Figure 3C). However, KH1* and KH2* granules recovered more rapidly ($t_{1/2}$ =
186 4.3 and 13.1s) suggesting these foci are much more dynamic than WT-FMRP (Figure 3A-
187 B and 3D). Collectively, these data indicate that the individual KH mutations decrease the
188 stability of FMRP in the mobile fraction. Finally, we examined the effect of removing or
189 disrupting both KH domains. Compared to single mutants, KH1*KH2* significantly
190 reduced dFMRP in the mobile fraction to 66% suggesting a large shift of FMRP into the
191 non-dynamic immobile fraction (Figure 3C). Similar results were observed with the ΔKH
192 mutant, however, recovery time of FMRP in the mobile fraction was significantly increased
193 ($t_{1/2}$ = 98.7s) (Figure 3D). These results further suggest that disruption of both the KH
194 domains may lead to the strengthening of interactions or protein aggregation.
195

196 **FXS-causing mutations alter the liquid-like properties of stress granules**

197 In addition to neuronal granules (NGs), FMRP is a component of both SGs and
198 PBs in neurons (Lai *et al.*, 2020). Precisely how FMRP interacts with different populations
199 of granules has yet to be elucidated. We hypothesized that mutations in the KH domains
200 might disrupt the association of FMRP with these RNP populations. To study interactions
201 with SGs, we co-transfected S2R+ cells with GFP-tagged FMRP constructs and mCherry-
202 tagged Rasputin (Rin), the fly ortholog of G3BP1, a conserved marker for and modulator
203 of SG assembly (Tourriere et al., 2003). In concordance with previous studies,
204 overexpression of Rin induced SG formation in ~20% of unstressed transfected cells
205 (Figure 4A and 4D) (Tourriere *et al.*, 2003). Interestingly, we found that these Rin-positive

Figure 3: FXS-causing point mutants alter FMRP-granules dynamics in S2R+ cells

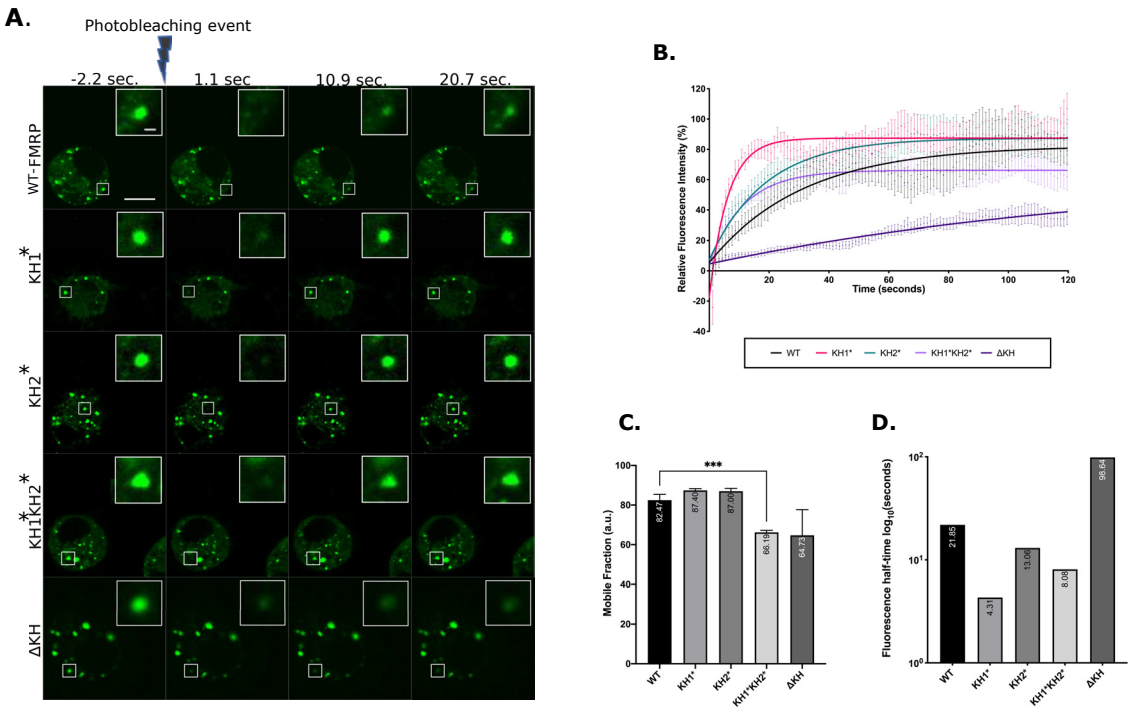

Figure 3: FXS-causing mutants alter FMRP granule dynamics in S2R+ cells
(A) Representative time-lapse FRAP images of FMRP-mutants pre- and post-bleaching. Scale bar in whole cell image = 5μm. Scale bar in zoomed-in granule image = 0.5μm. (B) Fluorescence recovery curves of FMRP-mutants over 120 seconds. Data points are mean ± SE. (C) Mobile fraction of FMRP mutant granules (mean ± SE; Brown-Forsyth test; ***$p<0.001$). a.u.=arbitrary units. (D) Quantification of the average time in $\log_{10}$(seconds), for granules to recover to half their final intensity ($t_{1/2}$). For B, C, and D n=17-21 granules.

Figure 4: FXS-causing mutations alter stress granule dynamics and P-body asssociation

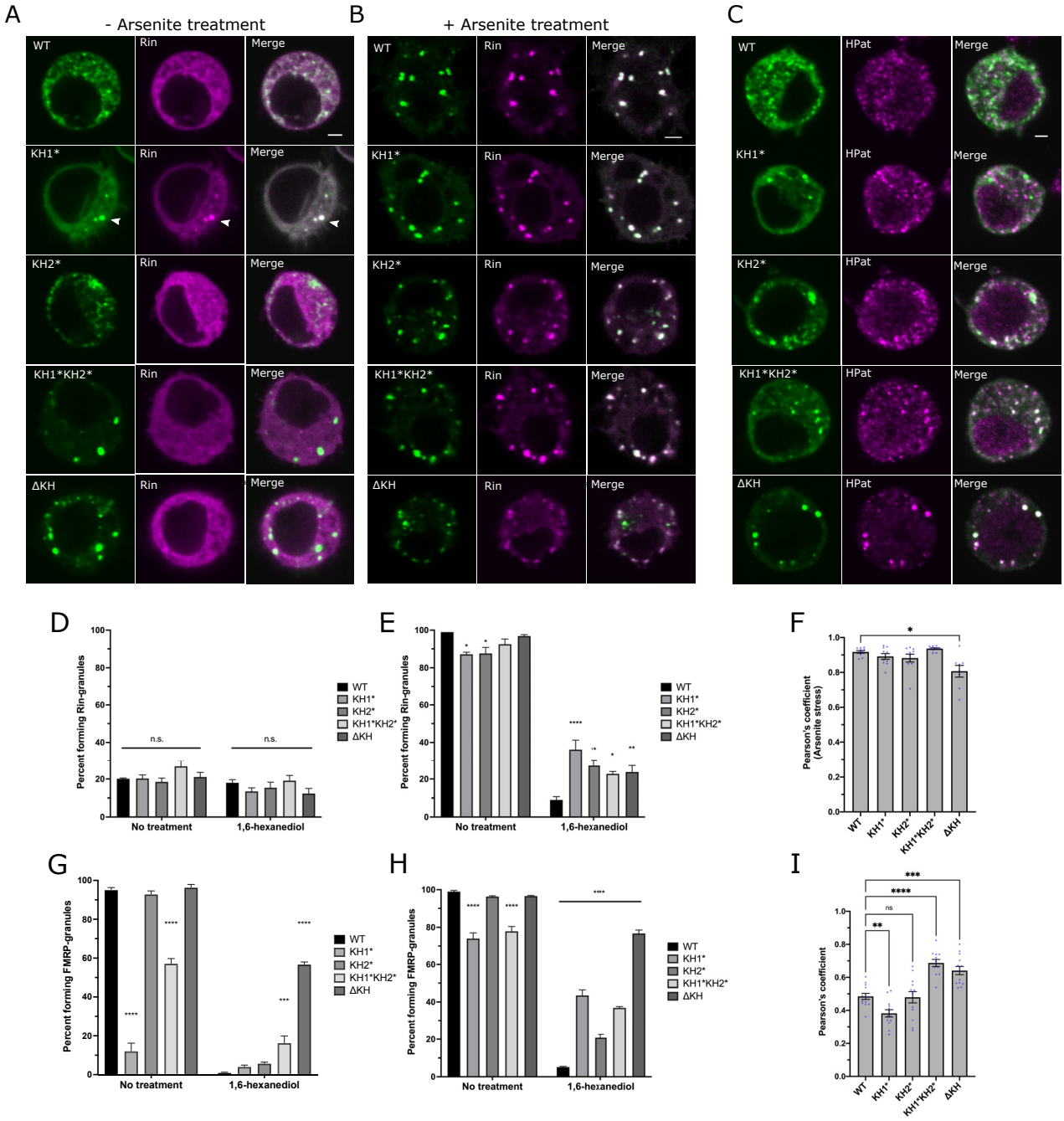

Figure 4: FXS-causing mutations alter SG dynamics and PB association
Representative images of S2R+ cells transfected with GFP-FMRP mutants (green) and Rin-mCherry (magenta) that are either not treated (A) or treated (B) with 0.5mM sodium arsenite for 45 minutes. Scale bars = 2μm. (C) Representative images of the localization of transiently transfected GFP-FMRP mutants immunostained against GFP (green) and HPat (magenta). Scale bar = 2μm. Percent of unstressed (D) or arsenite stressed (E) transfected cells forming Rin-positive SGs with or without 10% 1,6-HD treatment. Comparisons are made to WT-FMRP in each subcategory (mean ± SE; ~100 cells in triplicate; one-way ANOVA). (F) Average Pearson's correlation coefficient between FMRP-mutants and the stress granule marker, Rin, in arsenite treated cells (mean ± SE of 8-10 cells; Brown-Forsyth test). Percentage of unstressed (G) or arsenite stressed (H) transfected cells forming FMRP granules with or without 10% 1,6-HD compared to WT-FMRP (mean ± SE; ~100 cells in triplicate; one-way ANOVA). (I) Average Pearson's correlation coefficient between FMRP-mutants and HPat (mean ± SE of 12-13 cells; one-way ANOVA). In all graphs: * p<0.05, **p<0.01, ***p<0.001, ****p<0.0001.

206 granules always contained GFP-tagged FMRP and GFP-KH1* always colocalized with
207 Rin (Figure 4A). They were also resistant to treatment with 1,6-hexanediol (1,6-HD), an
208 aliphatic alcohol believed to interfere with weak protein-protein (π-π) and protein-RNA (π-
209 cation) interactions required to form liquid-like MLOs (Kroschwald et al., 2017) (Figure
210 4D). As expected, arsenite-induced stress triggered the formation of cytoplasmic SGs
211 (Figure 4B and 4E). Surprisingly, co-transfection with GFP-KH1* or GFP-KH2*
212 significantly reduced the number of cells that formed Rin-positive SGs (Figure 4E; left).
213 Moreover, the SGs that formed in cells co-transfected with KH mutants were more
214 resistant to 1,6-HD treatment then with WT-FMRP (Figure 4E; right). Together, this
215 suggests that the liquid-like nature of SGs is partially disrupted by the KH mutations.
216 Mammalian FMRP also accumulates in SGs under conditions of arsenite stress
217 (Kim et al., 2006). In concordance with these results, all GFP-tagged dFMRP constructs
218 colocalized strongly with Rin in stressed cells (Figure 4F). The number of cells containing
219 KH mutant granules also increased in stressed cells but those with KH1* and KH1*KH2*
220 were still significantly lower than WT-FMRP (Figure 4G-H; left). As with Rin, all KH mutant
221 granules in stressed cells were significantly more resistant to 1,6-HD compared to WT-
222 FMRP (Figure 4H; right). In the case of the KH1* and KH2* mutants, this was not likely
223 due to the persistence of pre-existing FMRP granules because these nearly disappear in
224 unstressed cells (Figure 4G; right). This further suggest that the liquid-like nature of SGs
225 has been disrupted by the single KH mutants. The presence of KH1*KH2* and ΔKH
226 granules in unstressed cells and their resistance to 1,6-HD treatment provides a third line
227 of evidence suggesting that these mutations are causing FMRP to aggregate.
228

229 **The KH1 domain is required for the localization of FMRP to P-bodies**

230 In addition to SGs, FMRP has been shown to colocalize with PB proteins in fly and
231 mammalian neurons (Barbee *et al.*, 2006; Cougot *et al.*, 2008). Thus, we were next
232 interested in determining if the KH mutants affected the ability of FMRP to interact with
233 HPat/Pat1p, a highly conserved PB protein that colocalizes with FMRP in *Drosophila*
234 neurons (Coller and Parker, 2005; Pradhan et al., 2012). To address this, we co-
235 transfected S2R+ cells with GFP-tagged FMRP constructs and immunostained against
236 HPat (Figure 4C). As expected, WT-FMRP overlapped moderately with HPat-positive
237 granules (Figure 4I). In comparison, colocalization was significantly reduced in KH1* and
238 most punctate GFP-KH1* failed to colocalize with punctate HPat (Figure 4C and 4I).
239 Taken together, these data suggest that the KH1 domain is required for the association
240 of FMRP with PBs. In contrast, KH1*KH2* and ΔKH caused the formation of larger
241 granules that strongly colocalized with HPat, suggesting that PB proteins are recruited to
242 these structures (Figure 4C and 4I). Based on these results and its propensity to form
243 solid-like aggregates, we excluded ΔKH from subsequent analyses in neurons.

244

245 **The KH1 domain is required for FMRP granule formation in primary neurons**

246 FMRP granules are important for the regulated trafficking of FMRP and specific
247 RNA cargos in axons and dendrites (Antar et al., 2004; Antar *et al.*, 2005; Antar *et al.*,
248 2006; Davidovic et al., 2007; Dictenberg *et al.*, 2008; El Fatimy *et al.*, 2016). Based on
249 our results in S2R+ cells, we asked if either of the KH domains played a role in the
250 assembly or dynamics of FMRP granules in neurons. We generated inducible GFP-
251 tagged dFMRP transgenic lines. First, we examined fly viability in a $dFmr1^{\Delta 50M}/dFmr1^{\Delta 113}$

252 (*Δ50/Δ*113) loss-of-function genetic background when transgenes were expressed in
253 larval motor neurons (*C380-Gal4, cha-Gal80* driver). As described, we found that the
254 *Δ50/Δ*113 allele combination was viable (Morales et al., 2002). Surprisingly, motor
255 neuron-specific expression of the GFP-KH1* and KH1*KH2* transgenes caused
256 embryonic lethality in *Δ50/Δ*113 mutant flies (data not shown). As a result, we conducted
257 all experiments below in a *Δ50/+* heterozygous background.

258 We next examined FMRP granules in 4-day old primary motor neuron cultures
259 from dissociated larval ventral ganglia. All cells expressing WT-FMRP formed generally
260 small, round granules in the soma (Figure 5A-B). In contrast, only 88% of cells expressing
261 KH2* formed granules and, like what we observed in S2R+ cells, they were less
262 numerous and sometimes formed amorphous structures (Figure 5A-B). Strikingly, GFP-
263 KH1* and KH1*KH2* formed few granules in the soma of only 2% and 10% of neurons
264 (respectively) suggesting that the KH1 domain is required to form FMRP granules *in vivo*
265 (Figure 5A-B). The level of expression of each KH mutant was similar, indicating that this
266 result was not likely due to reduced protein concentrations (Figure 5C). Both WT-FMRP
267 and KH2* granules were also found in neurites (Figure 5D). However, there were
268 significantly fewer GFP-KH2* granules outside of the soma (Figure 5D-E). Moreover,
269 fewer mutant granules were found in distal regions of neurites (Figure 5F). Together,
270 these data suggest that the KH2 domain is required for FMRP granule transport.

271

272 **The KH2 domain is required for FMRP granule trafficking in neurites**

273 We next asked if the KH mutations caused defects in the transport of FMRP
274 granules. As GFP-KH1* and KH1*KH2* do not form any granules in neurites (Figure 5A),

Figure 5: FXS-causing mutations in FMRP disrupt NG formation and dynamics in primary MNs.

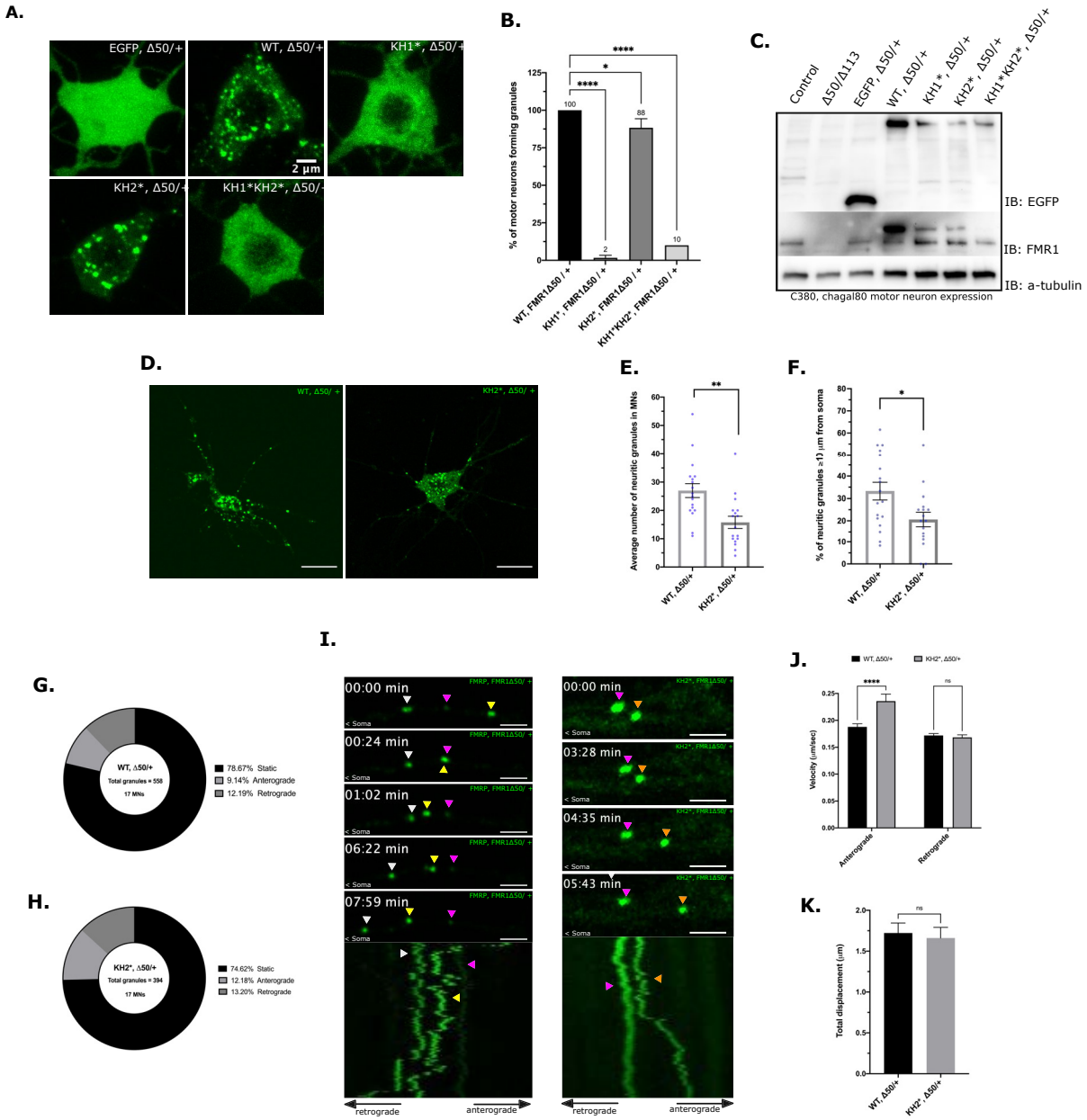

Figure 5: FXS-causing mutations disrupt NG formation and trafficking in neurons
(A) Representative images of major granule phenotype in primary neuron cell bodies. Expression of the indicated transgene was driven by *C380-Gal4, cha-gal80.* Scale bar = 2µm. (B) Percent of GFP-positive motor neurons forming FMRP granules in the *dFmr1$^{\Delta 50}$/+* background. Average is shown above respective bar (mean ± SE; 20 cells per triplicate, one-way ANOVA). (C) Western blot analysis of EGFP (top), FMRP (middle), and α-tubulin (bottom) expression under the *C380-Gal4, cha-gal80* selective motor neuron driver in the larval CNS. (D) Representative images of *WT, Δ50/+* and *KH2*, Δ50/+* primary MNs. Scale bar = 10µm. (E) Quantification of the average number of NGs within neurites of primary MNs (mean ± SE; 17-18 MNs, unpaired t test). (F) Percentage of neuritic granules that are distal (≥10 µm) from the MN cell body (mean ± SE; 17-18 MNs, unpaired t test). Pie charts representing the fraction of neuritic granules that remain stationary (static/oscillatory) or move in the anterograde or retrograde direction (relative to the cell body) in *WT, Δ50/+* (G) or *KH2*, Δ50/+* (H) primary neurons. Percentages are annotated in the legend for each chart (n= total granules in 17 MNs). (I) Time-lapse images and kymographs illustrating NG movements within neurites of WT (left panel) and KH2* (right panel) NGs. Images are oriented with the cell body on the left. Each granule is annotated with a colored arrowhead which corresponds with the traces in the kymograph. Scale bar = 2 µm. (J) Comparison of anterograde and retrograde velocities of motile WT-FMRP and KH2* NGs in neurites (mean ± SE; 46-75 granules per category; two-way ANOVA). (K) Average total displacement (µm) of all motile WT and KH2* NGs (mean ± SE; unpaired t test). In all graphs: * p<0.05, **p<0.01, ***p<0.001, ****p<0.0001.

275 we focused on *KH2*,Δ50/+* compared to *WT-FMRP,Δ50/+.* Consistent with recent
276 findings of GFP-tagged FMRP in hippocampal neuron dendrites, the majority of neuritic
277 WT-FMRP granules were stationary (Figure 5G) (El Fatimy *et al.*, 2016). Although, the
278 number of mobile granules in KH2 mutants was not significantly different, slightly more
279 KH2* granules were transported in the anterograde direction and the velocity of transport
280 was significantly increased (Figure 5H-J). Despite this increase in net velocity, total
281 granule displacement was not significantly altered (Figure 5K). These data, in conjunction
282 with the reduction in the number of FMRP granules found in distal neurites (Figure 5D-F),
283 suggest that the KH2 mutant granules have significant transport defects.
284

285 **The KH2 domain regulates the dynamics of FMRP in neuronal granules**

286 We next performed FRAP analysis in primary *Drosophila* motor neurons, looking
287 at somatic and neuritic granules as two separate populations (Figure 6A-D). In agreement
288 with published results, the mobile fraction of WT-FMRP was significantly lower in both the
289 soma and neurites (33% and 35% respectively) of cultured neurons than in S2R+ cells
290 (82%) suggesting that a larger proportion of WT-FMRP in NGs is found within the non-
291 dynamic, immobile fraction (Figure 6E and 3C) (Estes et al., 2008; Gareau *et al.*, 2013b).
292 While the size of the immobile fraction of NGs in both compartments was similar, the
293 recovery time of WT-FMRP in the mobile pool was about 2-fold slower in neuritic granules
294 ($t_{1/2}$ = 75s) than in those found in the soma ($t_{1/2}$ = 37s) (Figure 6E-F). Additionally, both
295 had slower recovery times than what we saw in S2R+ cells (Figure 3C-D). Together, these
296 data suggest that wild-type FMRP granules in neurons are less dynamic than those that
297 form in S2R+ cells. There were two observations with GFP-KH2* granules that support

Figure 6: FXS-causing mutations in FMRP disrupt NG dynamics in primary MNs.

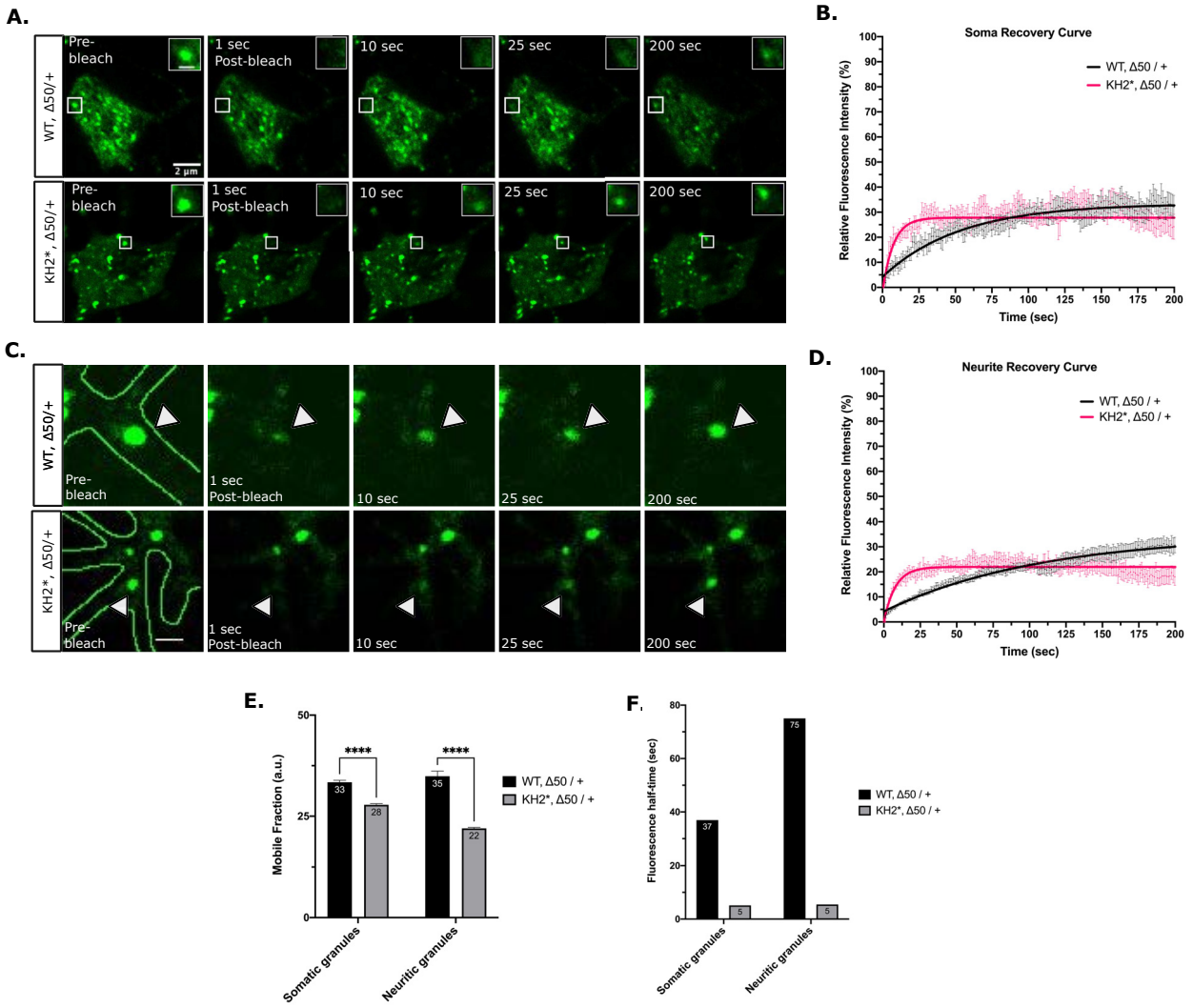

Figure 6: FXS-causing mutations in FMRP disrupt NG dynamics in neurons
(A) Representative FRAP time lapse images of somatic NGs pre- and post-bleaching event. Scale bar in whole cell images = 2 µm. Scale bar in zoomed-in granule images = 1 µm. (B) Fluorescence recovery curves of somatic NGs over 200 seconds (mean ± SE; n ≥ 9 granules). (C) Representative FRAP time-lapse images of neuritic NGs pre- and post-bleaching event. Neurites are outlined in green in the pre-bleach image, arrow heads point to the bleached granule. Scale bar = 1µm. (D) Fluorescence recovery curves of neuritic NGs showing fluorescence intensity relative to the initial pre-bleach intensity over 200 seconds (mean ± SE; n ≥ 13 granules). (E) Quantification of the average mobile fractions of somatic (left) or neuritic (right) mobile fraction of WT and KH2* NGs. a.u.=arbitrary units; $p < 0.0001$. (F) Quantification of the fluorescence half-time ($t_{1/2}$) of somatic or neuritic WT and KH2* NGs in seconds. For E and F n ≥ 9 granules.

298 the conclusion that this mutation alters FMRP granule dynamics in neurons. First, the
299 amount of KH2* found in the mobile fraction was significantly smaller in both somatic and
300 neuritic NGs (Figure 6E). Second, the recovery time of KH2* in the mobile fraction was
301 reduced ($t_{1/2}$ = 5s) (Figure 6F). These data further indicate that the composition and
302 dynamics of FMRP granules have been significantly altered by the KH2 mutation and
303 suggest that the KH domains are required to stabilize FMRP granules in neurons. Based
304 on these data, we propose that the disruption of this stability is contributing directly to the
305 transport defects seen in KH2* granules (Figure 5D-K).
306

307 **The KH domains are essential for the translational repression activity of FMRP**

308 We next wanted to examine the role of the KH domains in regulating the
309 translational repression activity of dFMRP. Both KH1* and KH2* have been shown to
310 disrupt the association of mammalian FMRP with polysomes suggesting that the KH
311 domains are important for translational repression (Darnell *et al.*, 2005; Feng *et al.*, 1997;
312 Myrick *et al.*, 2014; Zang *et al.*, 2009). Moreover, the KH domains of dFMRP bind directly
313 to the 80S ribosome and can block elongation *in vitro* (Chen et al., 2014). To further
314 examine the role of the KH domains in translational control, we used a λN-based tethering
315 assay in S2 cells, where the 3'UTRs of known dFMRP target mRNAs were fused to the
316 3' end of a firefly luciferase reporter, or FLuc (Figure 7A). To eliminate RNA binding as a
317 mechanism, we first tethered λN-tagged FMRP constructs directly to the reporter via a
318 5X tandem BoxB sequence that was inserted into the heterologous *SV40* 3'UTR. The
319 WT-FMRP and KH2* constructs were both able to repress translation (Figure 7B). In

Figure 7: FXS-causing mutations in FMRP affect FMRP functinon in translation and transport

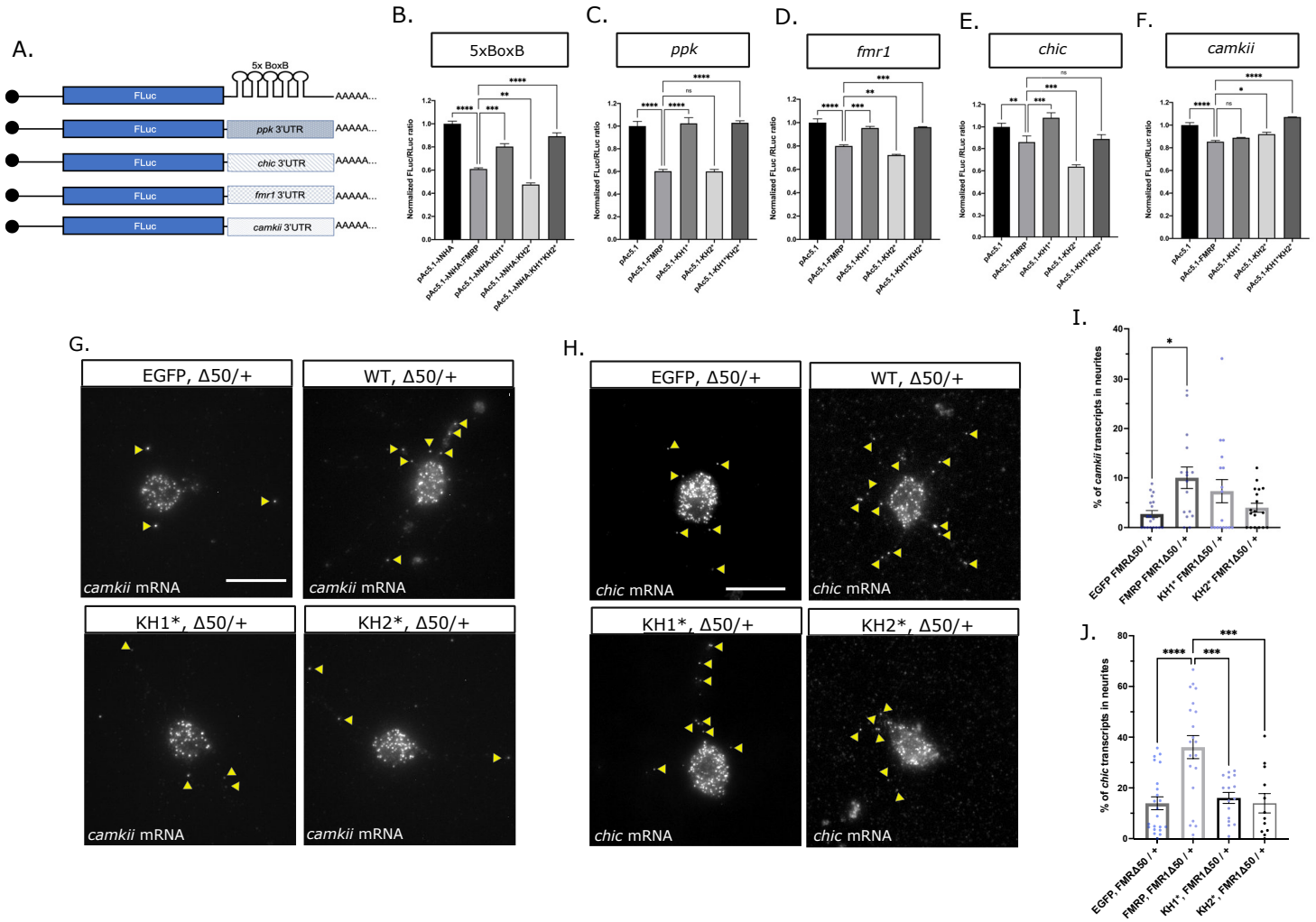

Figure 7: FXS-causing mutations disrupt translation and RNA transport

(A) Diagram of the FLuc reporters used in this study fused to the *SV40 3'UTR* containing the 5xBoxB sequence or to the 3'UTR's of known mRNA targets of dFMRP. Luciferase assays of (B) λN:HA-tethered FMRP-mutants repression of the 5xBoxB FLuc reporter or the untethered FMRP-mutants repression of FLuc fused to the (C) *pickpocket* (*ppk*), (D) *fmr1*, (E) *chickadee (chic)* or (F) *camkii* 3'UTR. FLuc/RLuc ratios were normalized to empty vector ratios. Graph shows repression of the FLuc reporter by empty vector or FXS-causing point mutants compared to *pAc5.1-λNHA:FMRP (B) or pAc5.1-FMRP (C-F)* (mean ± SE; one-way ANOVA). Representative images of *camkii* (G) or *chic* (H) mRNA smFISH in primary MNs. Yellow arrowheads in images are distinguishing transcripts found in neurites. Scale bars = 10μm. Quantification of the average number of *camkii* (I) or *chic* (J) transcripts in neurites of each of the FMRP mutants (mean ± SE of 11-25 MNs; unpaired t test). In all graphs: * p<0.05, **p<0.01, ***p<0.001, ****p<0.0001.

320 contrast, the ability of KH1* to repress reporter expression was significantly disrupted,
321 suggesting that the KH1 domain is required for repression activity.

322 Next, we determined whether untethered dFMRP could repress the translation of
323 Fluc by binding to the 3'UTRs of known targets mRNAs and if either of the KH domains
324 were required for this to occur. We replaced the *SV40* 3'UTR containing the BoxB repeats
325 with the 3'UTRs from mRNAs encoding for: 1) the degenerin/epithelial sodium channel
326 (DEG/ENaC) family member, *pickpocket* (*ppk*); 2) the Ca^{2+}/calmodulin-dependent protein
327 kinase II, *camkii*; 3) the profilin ortholog, *chickadee (chic)*; and 4) its own mRNA, *fmr1*
328 (Reeve et al., 2005; Sudhakaran et al., 2014; Xu et al., 2004; Zhang *et al.*, 2001) (Figure
329 7A). As with the BoxB reporter, the KH1 domain was required to regulate repression of
330 the *ppk*, *chic,* and *fmr1* reporters as repression was ameliorated in KH1* and KH1*KH2*
331 (Figure 7B-E). The efficiency of repression of each of these reporters by WT-FMRP and
332 KH2* was variable, likely due to differences in the ability of these proteins to interact with
333 or bind to the 3'UTR. In contrast, the *camkii* reporter was different in that repression is
334 slightly but significantly derepressed by KH2* and KH1*KH2* indicating that the KH2
335 domain is required for repression (Figure 7F). Collectively, these data indicate that FXS-
336 causing mutations in the KH1 and KH2 domains can differentially regulate translational
337 repression. The derepression of translation in KH1* correlates with defects in its ability to
338 form FMRP granules in cells and neurons (Figure 2 and 5).

339

340 **The KH domains are required for the transport of FMRP target RNAs**

341 NGs are specialized MLOs within neurons that serve to transport translationally
342 silent mRNAs between the soma and axonal or dendritic compartments (Formicola et al.,

343 2019). Therefore, we next asked if *KH1*,Δ50/+* or *KH2*,Δ50/+* neurons had defects in
344 mRNA localization. To address this, we used single-molecule fluorescence *in situ*
345 hybridization (smFISH) to quantify transcripts in the soma and neurites. We focused on
346 two mRNA targets of dFMRP in flies, *chic* and *camkii*, both of which have been shown to
347 interact with dFMRP-containing NGs in primary motor neurons (Barbee *et al.*, 2006; Estes
348 *et al.*, 2008). Their translational repression is also regulated by the KH1 and KH2 domains
349 (Figure 7E-F). We find that there are significantly more *camkii* and *chic* transcripts in *WT-*
350 *FMRP,Δ50/+* neurites compared to controls suggesting that dFMRP promotes the
351 transport of both mRNAs to neurites (Figure 7G-J). The percentage of *chic* transcripts
352 found in neurites is significantly reduced in both KH1* and KH2*. In contrast, localization
353 of *camkii* is not affected by either mutation. Taken together, these data suggest that the
354 *chic* and *camkii* mRNAs are differentially localized to neurites through a KH domain-
355 dependent and independent mechanism (respectively).
356

357 **DISCUSSION**

358 FMRP has been implicated in a growing number of biological processes in neurons
359 ranging from the control of translation and RNA transport to the regulation of RNA editing,
360 splicing, genome stability, and ion channel function (Davis and Broadie, 2017). Because
361 the vast majority of FXS cases are caused by loss of FMRP expression, it has been
362 difficult to determine which of these functions are involved in FXS pathophysiology. In
363 contrast, the study of disease-causing missense mutations in FMRP has allowed for the
364 isolation of specific protein functions that may be contributing to FXS phenotypes (Suhl
365 and Warren, 2015). Here, we provide multiple lines of evidence that FXS-causing

366 mutations in the KH domains differentially affect FMRP granule assembly, dynamics, and
367 function in *Drosophila* neurons. First, an FXS-causing missense mutation in the KH1
368 domain disrupts the ability of FMRP to form granules in primary neuron cell culture (Figure
369 5A-B). In contrast, KH2 mutants form granules in the soma but their transport to distal
370 neurites is reduced (Figure 5D-F). Second, we find that KH2* significantly decreases the
371 amount and stability of FMRP found in the mobile fraction of neuronal FMRP granules
372 (Figure 6E-F). Third, the KH domains are differentially required to regulate the translation
373 of reporters for known target mRNAs (Figure 7B-F). Finally, both KH domains promote
374 the localization of specific target mRNAs to neurites (Figure 7G-J). Translational
375 repression and RNA transport are processes that have been directly attributed to FMRP-
376 containing RNA granules in neurons (Richter and Zhao, 2021).

377 The disordered C-terminus of mammalian FMRP is necessary and sufficient to
378 drive the formation of phase-separated droplets *in vitro* (Tsang *et al.*, 2019). Furthermore,
379 phosphorylation patterns of amino acids in this region control the propensity to phase
380 separate in the presence of RNA and to regulate rates of deadenylation and translation
381 within these condensates (Kim et al., 2019). Collectively, these data suggest that
382 regulation of FMRP phase separation might be a simple mechanism to allow for the
383 delivery of translationally repressed mRNAs to synapses and to control their local
384 translation in response to activity. Through our analysis of *Drosophila* FMRP granules in
385 cells, we show that the C-terminal IDR is sufficient to regulate granule formation (Figure
386 1D). However, granule formation is significantly enhanced by the addition of the
387 structured KH domains (Figure 1D). This is consistent with current models suggesting
388 that MLO formation *in vivo* is driven by multivalent interactions between protein and RNA

389 components (Mittag and Parker, 2018; Van Treeck and Parker, 2018). Increased valency
390 provides a scaffold of *cis*-acting binding sites that allow for interactions with multiple *trans*-
391 acting partners, allowing interacting molecules to compartmentalize within the cell
392 (Banani et al., 2016; Li et al., 2012). Published findings also show that different types of
393 NGs are generally more stable than other types of MLOs (Chae et al., 2010; Cougot *et*
394 *al.*, 2008; Formicola *et al.*, 2019; Gopal et al., 2017; Vijayakumar et al., 2019). In support
395 of this, we find that WT-FMRP granules are significantly less dynamic in primary neurons
396 than in S2R+ cells (Figure 3 and 7). This stability is likely to be necessary so that FMRP
397 granules can resist the shear stress associated with active transport.

398 While the precise RNA binding sites are a source of debate, the KH domains
399 clearly bind with different specificity and/or affinity to target mRNAs (Athar and Joseph,
400 2020). Therefore, the simplest explanation for the role of the KH domains in regulating
401 FMRP granule formation and dynamics is that they are increasing valency through
402 interactions with RNA. Why does the KH1 mutation have a more significant impact on
403 FMRP granules? It is possible that the KH1 domain is contributing disproportionately
404 strong (or numerous) interactions with mRNAs which is shifting the critical concentration
405 needed for granule formation. Interactions occurring via KH1 could be shifting the
406 concentration threshold required to promote FMRP granule formation. For example,
407 multivalent interactions between RNA and proteins such as hnRNPA1 and FUS, influence
408 LLPS by shifting the phase boundary and requiring lower protein concentrations to initiate
409 demixing (Molliex et al., 2015; Schwartz et al., 2013; Tsang *et al.*, 2019).

410 Our analysis of KH domain function also reveals a link between FMRP granule
411 formation and translational repression in neurons. A significant fraction of mammalian and

412 *Drosophila* FMRP interacts with polysomes and this association is disrupted by the
413 G266E and I304N mutations (Feng *et al.*, 1997; Ishizuka et al., 2002; Myrick *et al.*, 2014;
414 Zang *et al.*, 2009). One mechanism by which FMRP blocks translation is by interacting
415 with stalled polysomes (Darnell et al., 2011). More specifically, the KH domains of dFMRP
416 interact directly with the peptidyl site of ribosomes (Chen *et al.*, 2014). This suggests a
417 mechanism by which FMRP stalls translational elongation by sterically inhibiting tRNA
418 entry. The non-disease associated KH1 mutant (I244N) and KH2* (I307N) both disrupt
419 binding affinity, with the I244N mutation having a stronger effect (Chen *et al.*, 2014).
420 Interestingly, analysis of FMRP granules in mouse brain homogenates by electron
421 microscopy found that FMRP and ribosomes both localize to a subset of neuronal RNA
422 transport granules (El Fatimy *et al.*, 2016). These data led the authors to propose that
423 FMRP granules form from stalled polysomes. A prediction from this model is that
424 disruption of FMRP-ribosome association would negatively impact the formation of a
425 subset of FMRP granules. Our data provide support for this model as we show that KH1*
426 and KH2* both disrupt FMRP granules, with the KH1 mutant having a stronger effect
427 (Figure 2C-D and 5A-B). We also demonstrate that the KH1 domain is required to repress
428 the translation of most translational reporters tested, including when FMRP was directly
429 tethered to a heterologous 3'UTR (Figure 7B-E). Additional studies would be required to
430 determine if there is a direct connection between polysomes, ribosome stalling, and
431 FMRP granule formation in *Drosophila* neurons. This would also help to clarify whether
432 FMRP granules are a cause or consequence of translational repression.

433 In cultured mouse neurons, the specificity of FMRP for mRNAs targeted for
434 transport to neurites is conferred by interactions between its C-terminal RGG domain and

435 G-quadraplex sequences within the 3'UTRs of localized mRNAs (Goering et al., 2020).
436 This study also found that the FXS-causing KH2 mutant (I304N) which disrupts ribosome
437 association retained the ability to promote the localization of G-quadraplex-containing
438 transcripts to neurites. In contrast, we show that both the KH1 and KH2 mutants fail to
439 promote the localization of *chic* (but not *camkii*) to neurites in cultured *Drosophila* neurons
440 (Figure 7G-J). The long *chic* 3'UTR (but not *camkii*) contains G-rich sequences predicted
441 to fold into quadraplexes (data not shown) suggesting that localization of these fly mRNAs
442 may be regulated by a G-quadraplex-independent mechanism. This might be due to our
443 limited sample size as mouse studies focused on a global analysis of mRNA localization
444 (Goering *et al.*, 2020). Alternatively, the control of mRNA transport by *Drosophila* FMRP
445 may be mechanistically different. The RGG domain found in dFMRP is not highly
446 conserved and it fails to bind with high affinity to the *sc1* RNA, a G-quadraplex-containing
447 target for human FMRP (Darnell et al., 2009). Unlike in mouse studies, we also observe
448 both transcript- and KH domain-specific coupling of translational repression and mRNA
449 localization in *Drosophila* neurons (Figure 7) (Darnell *et al.*, 2009). It is possible that this
450 represents a *bona fide* difference between fly and mammalian FMRP.

451 The role of FMRP granules in the transport and translation of target mRNAs in
452 neurons is complex because their organization, dynamics, and function are regulated by
453 multivalent interactions involving both structured and unstructured protein domains. Our
454 data support a model where FMRP granules are metastable, solid-like, MLOs. This is a
455 state that is likely necessary to allow for their active transport in neurites without the loss
456 of RNA and protein components. We demonstrate that the KH1 and KH2 domains are
457 required to maintain FMRP granule integrity in both S2R+ cells and neurons. FXS-causing

458 mutations disrupt this equilibrium, leading to the formation of MLOs that are unstable.
459 This is distinctly different from disease-causing mutations in IDR-containing RBPs that
460 have been linked to neurodegenerative disease such as TDP-43, FUS, or hnRNP-A1,
461 which lead to the formation of metastable, then stable, pathological inclusions (Molliex *et*
462 *al.*, 2015; Patel et al., 2015). That said, our studies have revealed novel granule
463 phenotypes associated with FXS-causing KH mutations. First, both KH mutations disrupt
464 the sensitivity of SGs to 1,6-HD, suggesting that their biophysical properties have been
465 altered (Figure 4D-H). KH1* has a more significant impact on this phenotype than KH2*.
466 Second, MN-specific genetic "rescue" experiments with KH1* causes lethality in an
467 otherwise viable *dFmr1* loss-of-function background suggesting that G266E may be an
468 uncharacterized gain-of-function mutation (data not shown). Finally, the KH1 mutation
469 also nearly abolishes FMRP granule formation in neurons. These results may explain why
470 the G226E mutation causes such a severe form of FXS (Myrick *et al.*, 2014).
471

472 **METHODS**

473 **Fly stocks and husbandry**

474 In all experiments, both male and female flies were used. All lines were incubated
475 at 25°C with 12-hour light/dark cycles and 60% humidity on standard Bloomington
476 medium. Fly lines used and made in this study are listed in Table S1. Plasmid constructs
477 for the generation of transgenic lines were constructed as described below. All transgenes
478 were injected into fly strain 24485 for *PhiC31*-mediated integration into the same site on
479 chromosome III. All transgenes were recombined with the $dFmr1^{\Delta 50M}$ null allele.
480

481 **Cell culture**

482 S2 and S2R+ cells were maintained at 24°C with ambient humidity in a dark
483 incubator in M3+BPYE media. S2-DRSC cells were used for luciferase reporter assay
484 experiments. S2R+ cells were used for imaging experiments due to their higher
485 propensity to adhere to and flatten out on poly-D-lysine coated cover slips. Cells and
486 media recipes were obtained from the *Drosophila* Genomics Resource Center (DGRC).
487 Primary motor neurons were cultured from wandering 3rd instar larvae using a protocol
488 adapted from Barbee et al. 2006. For each genotype, ventral ganglia from ten third instar
489 larvae were dissected, dissociated, and then grown in complete M3+BPYE media
490 (M3+BPYE supplemented with 50 µg/mL insulin) for 3 to 5 days prior to imaging.

491

492 **Cloning and site directed mutagenesis**

493 The backbone vector for all S2 cell culture plasmids is a modification of pAc5.1
494 (ThermoFisher Scientific, Waltham, MA) which drives expression from the fly actin 5C
495 gene. For imaging of FMRP, the coding region of the *FMR1-RD* cDNA (LD09557; DGRC)
496 was PCR amplified and cloned downstream of EGFP in the pAc5.1B-EGFP vector (a gift
497 from Elisa Izaurralde; Addgene plasmid #21181) using the *HindIII* and *EcoRI* restriction
498 sites to make pAcB5.1-EGFP-FMRP. The pAc5.1:EGFP-FMRP-IDR, pAc5.1:EGFP-
499 FMRP-ΔIDR, pAc5.1:EGFP-FMRP-KH:IDR and pAc5.1:EGFP-FMRP-ΔKH plasmids
500 were all constructed by PCR amplification of the indicated sequence followed by cloning
501 into pAc5.1B-EGFP. Primer sequences and restriction sites are listed and described in
502 Table S2. The *Drosophila* G269E and I307N mutations were generated using the Q5 Site-
503 Directed Mutagenesis Kit (New England Biolabs, Ipswitch, MA). Mutagenesis primers

504 were designed using the “substitution” feature in NEBaseChanger v1.2.9 (New England
505 Biolabs). Mutagenesis occurs at nucleotide 805-807 (GGA→ GAA) and nucleotide 868-
506 870 (ATC→ AAC) in the KH1 and KH2 domain, respectively. Each mutation was
507 introduced directly into the pAc5.1B:EGFP-FMRP vector. The KH1*KH2* double mutant
508 was created by introducing both mutations sequentially (KH1* followed by KH2*).

509 Plasmids for the generation of transgenic fly lines were all constructed as follows.
510 The EGFP-FMRP sequence for WT-FMRP and each mutant construct were PCR
511 amplified from their respective pAc5.1 vector using primer sequences listed and
512 described in Table S2. Products were then cloned directionally into the 5’-*KpnI* and 3’-
513 *XbaI* sites of pUAST-attB. Transgenic flies were generated as described above.

514 To construct the pAc5.1-Rin-mCherry plasmid, we first generated a pAc5.1B-MCS-
515 $(Gly_4Ser)_3$-mCherry plasmid. The Rin cDNA was obtained by reverse-transcriptase PCR
516 from RNA extracted from wild-type (*CantonS*) adult flies. Total RNA was extracted using
517 the Direct-zol RNA kit (Zymo Research, Irivne, CA) and cDNA was generated using the
518 RNA to cDNA EcoDry™ Premix Oligo dT kit (Takara Bio USA, Moutain View, CA). Rin
519 was PCR amplified using primers listed and described in Table S2 and cloned into the
520 *HindIII* and *EcoRI* restriction sites of pAc5.1-MCS-$(Gly_4Ser)_3$-mCherry to generate the
521 final pAc5.1:Rin-$(Gly_4Ser)_3$-mCherry vector.

522 To construct plasmids for the tethered FLuc reporter assays, the wild-type dFMR1
523 and KH1*, KH2*, or KH1*KH2* mutants were PCR amplified from their respective
524 pAc5.1B-EGFP vector and cloned into the *HindIII* and *EcoRI* sites of the pAc5.1-
525 lambdaN-HA vector (a gift from Elisa Izaurralde; Addgene plasmid #21302) (Behm-
526 Ansmant et al., 2006). For the untethered reporter assays, the indicated dFMR1

527 constructs were cloned into the MCS of pAc5.1B lacking the lambdaN-HA tag. The BoxB
528 reporter was pAc5.1C-Fluc-Stop-5BoxB (a gift from Elisa Izaurralde; Addgene plasmid
529 #21301) (Behm-Ansmant *et al.*, 2006). To construct the *camkii* and *Fmr1* reporters, the
530 *SV40* 3'UTR and the 5xBoxB sequence was removed by digesting pAc5.1C-Fluc-Stop-
531 5BoxB with *EcoRI* and *XhoI*. The long 3'UTR isoform of *camkii* and *Fmr1* were amplified
532 by RT-PCR (as described for Rin) using primers listed and described in Table S2. The
533 3'UTRs were then cloned into the cut plasmid via Gibson Assembly using the Gibson
534 Assembly Master Mix (New England Biolabs). The 3'UTRs of *ppk* and *chic* were amplified
535 by RT-PCR, cloned into pENTR D-TOPO, and into the pAc5.1-FLuc2 [dPolyA] RfA
536 destination vector as we have previously described (Nesler et al., 2013).
537

538 **S2 cell transfections**

539 DNA transfections were performed with the Effectene Transfection Reagent kit
540 (Qiagen). Transient transfections were performed following the manufacturer's protocols.
541 For fluorescence experiments, DNA constructs were transfected into S2R+ cells in 12-
542 well plates. Cells were transfected with 0.5 µg of each construct except for pAc5.1B-
543 EGFP:FMRP:KH1* in which 0.75 µg of DNA was used. Transfected cells were grown for
544 ~ 72 hours before imaging. For luciferase assays, S2-DRSC cells in 24-well plates were
545 transfected with 0.025 µg of the FLuc reporter plasmid, 0.1 µg of the *Renilla* luciferase
546 (RLuc) transfection control plasmid, and 0.25 µg of either the pAc5.1/pAc5.1-λN control
547 vector or the pAc5.1:FMRP/pAc5.1-λN:FMRP wild-type or mutant constructs. Transfected
548 cells were grown for ~ 72 hours prior to analysis in luciferase experiments.
549

550 **S2 cell imaging and granule analysis**

551 S2R+ cells were transferred to poly-D lysine coated #1.5 cover glass bottom dishes
552 (Cellvis, Mountain View, CA) within two hours of imaging. In all experiments, images were
553 obtained using an Olympus FV3000 scanning confocal microscope with a 100x (NA 1.4)
554 objective digitally zoomed to 2.95x (the optimal setting per the Fluoview software). To
555 quantify the number of granules formed by each construct, 15 cells were analyzed in a
556 single experiment. The single z-plane where the nucleus took up the largest cell area was
557 imaged. Punctate areas of fluorescence intensity above background were considered to
558 be granules and were quantified using the Cell Counter plugin in ImageJ2/FIJI. For each
559 image, cell diameter (through the longest axis in the same z-plane) and granule number
560 were collected. From this, the number of granules per cell area (μm^2) was recorded. To
561 count the number of transfected cells able to form granules, ~ 100 cells per FMRP
562 construct were manually identified at the microscope. The total number of cells that
563 formed granules out of all EGFP-expressing cells were quantified. Cells were scanned in
564 z to make sure that granules in all planes were identified. The number of cells that formed
565 granules was divided by total number of transfected cells for three separate experiments.
566 To compare the propensity of the different mutants to form circular granules, ~ 100
567 granule forming transfected cells were identified at the microscope. The number of cells
568 forming circular and amorphic (non-circular) granules were counted. In most cases, cells
569 that formed amorphous granules also contained circular granules, however, cells that
570 formed any number of amorphous granules were categorized as amorphic.

571

572 **Fluorescence Recovery After Photobleaching (FRAP) experiments**

573 For all FRAP experiments, 17-21 EGFP positive granules were imaged using an
574 Olympus FV3000 scanning confocal microscope with a 100x (NA 1.4) objective digitally
575 zoomed to 2.95x (optimal settings). Granules selected for FRAP analysis generally fit into
576 the “spherical” category. Granules selected for analysis in primary neurons were clearly
577 in the cell body or neuritic compartments. In all cases, granules were photobleached with
578 the lowest laser intensity necessary to completely bleach the granule, ranging from 2.44-
579 10% 488nm laser power for 500-1,000 milliseconds. Two pre-FRAP images were
580 collected and images were captured every 1.0878 seconds pre and post bleaching for a
581 total of 200 frames (~ 218 s). For image analysis, images were initially processed in
582 ImageJ2/FIJI) and analyzed essentially as described (Cheney et al., 2017). A ROI was
583 manually traced in each FRAP movie for 1) the bleached granule, 2) an unbleached
584 granule and 3) diffuse cytoplasmic staining for background. As necessary, the ROI was
585 moved if/when granules moved in x/y out of the initially set ROI. If a granule clearly
586 dropped out of the focal plane, it was excluded from analysis. The mean fluorescent
587 intensity was obtained for each frame. The following was calculated: 1) Photobleach
588 Correction Value (PCV), in which the average intensity of the pre-bleach unbleached
589 granule was divided by the value for each subsequent unbleached granule, 2) Corrected
590 Average Intensity (CAI), where the bleached granules mean intensity was multiplied by
591 the PCV, 3) Background Corrected Fluorescence Intensity (BCFI), where the CAI was
592 subtracted by the average intensity of the background ROI, and 4) the Final Corrected
593 Value (FCV) which was calculated by dividing each BCFI by the initial BCFI value and
594 multiplying by 100 to get a normalized fluorescence intensity profile. The FCVs from each

595 movie were then analyzed a one-phase association, nonlinear fit in Graphpad Prism to
596 calculate the fluorescence recovery curve, mobile fraction, and half-life.
597
598 **Immunocytochemistry**
599 S2R+ cells were transferred to poly-D lysine coated #1.0 cover glass bottom dishes
600 (Cellvis) and allowed to settle for ~ 20 minutes. Cells were then fixed with 4% PFA for 10
601 minutes followed by a 5-minute incubation in ice cold methanol. Cells were washed three
602 times for 5 minutes in PBS, permeabilized in PBST for 10 minutes, and then blocked in
603 PBST with 2% BSA and 5% normal goat serum for 30 minutes. Cells were then incubated
604 with primary antibodies overnight at 4°C, washed three times for 5 minutes in PBS, and
605 then incubated for 1 hour in secondary antibodies at room temperature. Finally, cells were
606 washed with PBS and then mounted in DAPI-Fluoromount-G Clear Mounting Media
607 (ThermoFisher Scientific). EGFP:FMRP constructs were visualized by GFP fluorescence.
608 For HPat, rabbit anti-HPat (1:1,500) (Pradhan *et al.*, 2012) primary and goat anti-rabbit
609 Alexa-567 (1:500) secondary antibodies were used.
610
611 **Arsenite and 1,6-hexanediol treatment**
612 For SG experiments, cells were co-transfected with the indicated pAc5.1B:EGFP-
613 FMRP construct and pAc5.1-Rin-mCherry. About 72 h post transfection, cells were
614 treated with 0.5mM sodium arsenite in M3+BPYE media for 45 minutes to induce SG
615 formation. Non-stressed cells went through the same procedure but were incubated in
616 media that did not contain sodium arsenite. For colocalization analysis, cells were
617 immediately fixed in 4% PFA for 10 minutes, incubated with ice cold methanol for 5

618 minutes and then washed 3 times for 5 minutes in PBS. Preparations were then mounted
619 on coverslips as described above. FMRP and Rin were visualized by imaging GFP and
620 mCherry fluorescence respectively. For the analysis of granules with treated with 1,6-HD,
621 cells were co-transfected with pAc5.1:EGFP-FMRP constructs and pAc5.1-Rin-mCherry.
622 Cells were subjected to arsenite stress (or not stressed) as described above. Following
623 the 45-minute incubation (+/- sodium arsenite), cells were treated with M3+BPYE media
624 (+/- sodium arsenite) containing 10% 1,6-HD. Approximately 100 live transfected cells
625 were analyzed for the presence or absence of FMRP or Rin granules, in triplicate.
626

627 **Colocalization analysis**

628 To determine the degree to which FMRP mutants colocalized with SGs or PBs,
629 12-13 images were analyzed in ImageJ2/FIJI using the JACoP plugin (Bolte and
630 Cordelieres, 2006). Images were cropped to the smallest area possible to eliminate
631 colocalization outside of the cell of interest and images for FMRP/HPat were background
632 subtracted to a rolling ball radius of 50 pixels to account for the higher degree of HPat
633 background staining. In JACoP, Pearson's coefficient results were recorded for analysis.
634

635 **Western blotting**

636 For the detection of EGFP-FMRP construct levels in S2R+ cells, transfected cells
637 were harvested at three days post-transection from a 6-well plate. Cells were scraped
638 and resuspended by pipetting up and down and 1.5 mL of cells were spun down at 1,000x
639 G for 5 minutes at 4°C. Cells were then resuspended in 400 µL of 2x Laemmli sample
640 buffer + **β**-mercaptoethanol on ice. For westerns conducted on *C380, cha-Gal80/+ ;*

641 *UAS:EGFP-FMRP, FMR1$^{\Delta 50M}$/+* larvae ectopically expressing the wild-type and FXS-
642 causing point mutants, 5 ventral ganglia (including optic lobes) were dissected and added
643 to 100μL of 2x Laemmli sample buffer + **β**-mercaptoethanol on ice. Then, the ventral
644 ganglia were homogenized in a 1.6 mL microcentrifuge tube for 30 seconds on ice using
645 a hand-held homogenizer. Homogenates were incubated on ice for 3 minutes, and then
646 processed as indicated above for S2R+ cells. For both assays, the primary antibodies
647 used were mouse anti-dFMR1 (1:3,000; 6A15; Abcam, Cambridge, UK), rabbit anti-EGFP
648 (1:2,000; Proteintech Group, Rosemont, IL), and mouse anti-α-tubulin (1:1,000; 12G10;
649 Developmental Studies Hybridoma Bank, Iowa City, IA). Secondary antibodies used were
650 horse anti-mouse HRP or goat anti-rabbit HRP which were both diluted 1:1,000 in block
651 (Cell Signaling Technology, Danvers, MA).
652

653 **Primary motor neuron imaging and neurite transport analysis**

654 For analysis of *C380, cha-Gal80/+ ; UAS:EGFP-FMRP, FMR1$^{\Delta 50M}$/+* larvae
655 expressing either wild-type FMRP or the KH2 mutant, primary larval motor neurons were
656 collected and cultured as described above. At 4 days post-harvest, live neurons were
657 imaged using an Olympus FV3000 scanning confocal microscope with a 100x (NA 1.4)
658 objective. For soma imaging, images were digitally zoomed to 2.95x for optimal resolution
659 and a z-stack was obtained with 0.39μm slices through the entire soma. Images were
660 presented as Z-projections made using ImageJ2/FIJI. For neurite transport analysis, live
661 cells were imaged with a 100x objective (NA 1.4) digitally zoomed to 1.79x so branching
662 neurites could be imaged. Movies were collected containing four 0.39μm z-slices, over
663 100 frames (8:04 minutes). Movies were then analyzed using the Kymolyzer plugin in

664 ImageJ2/FIJI from which granule velocities and directionality were obtained, using a lower
665 speed limit set to the pixel size (0.138μm) (Basu et al., 2020). To calculate the average
666 number of neuritic granules in primary motor neurons, the max-intensity Z-projection of
667 the first time point was used (Frame 1). The number of granules in the soma and neurites
668 were manually counted using the Cell Counter plugin for ImageJ2/FIJI. Additionally, the
669 proportion of neuritic granules 10μm or further from the cell body was determined from
670 these images. The scale was globally set, and a symmetrical circle was drawn tightly
671 around each cell using the oval selection tool in ImageJ, containing as much of the cell
672 as possible. The diameter of each cell body was recorded in μm. The center of each circle
673 was determined and marked using the Pencil tool. A line was drawn to the center of each
674 granule within neurites and distance from the cell body was recorded in μm. These were
675 subtracted by the radius for their respective cell body to obtain the final distance.
676

677 **Luciferase reporter assays**

678 Luciferase reporter assays were done essentially as we have described (Nesler *et*
679 *al.*, 2013). At three days post transfection, 75 μL of resuspended cells were added in three
680 technical replicates to a 96-well white, flat bottom polystyrene assay plate (Costar,
681 Washington, DC). FLuc and RLuc expression was measured using the Dual-Glo
682 Luciferase Assay System kit (Promega, Madison, WI) per the manufacturer's instructions
683 and luminescence detected using a Synergy™ HTX Multi-Mode Microplate Reader
684 (BioTek, Winooski, VT). FLuc values were normalized to corresponding RLuc values. The
685 FLuc/RLuc ratio for each experiment was normalized to its respective control. The
686 experiment was repeated three times for each FLuc reporter.

687

688 **Single molecule FISH and FISH-quant image analysis**

689 For analysis of *C380, cha-Gal80/+ ; UAS:EGFP-FMRP, FMR1$^{\Delta 50M}$/+* larvae
690 expressing either wild-type FMRP or the KH2 mutant, primary larval motor neurons were
691 collected and cultured as described above. Custom Stellaris® FISH Probes were
692 designed against *Drosophila melanogaster camkii* and *chic* by utilizing the Stellaris® FISH
693 Probe Designer (Table S3; Biosearch Technologies, Hoddesdon, UK). Primary motor
694 neurons were hybridized with the indicated Stellaris FISH Probe set labeled with either
695 Quasar-570 or 670 (Biosearch Technologies) following the manufacturer's instructions.
696 Briefly, at 3-4 days post culturing, cells growing on #1.5 cover glass were washed in PBS.
697 Cells were then incubated in fixation buffer (3.7% formaldehyde in PBS) for 10 minutes
698 at room temperature, then washed twice in PBS. To permeabilize cells were immersed in
699 70% ethanol at 4°C for at least 1 hour and up to a week. Ethanol was aspirated and cells
700 were washed in Stellaris Wash Buffer A for 5 minutes, then hybridized with the indicated
701 probe(s) in a dark, humid hybridization chamber at 37°C for 5-16 hours. Probes were
702 used at a final molarity of 0.125μM in Stellaris Hybridization buffer. Hybridization buffer
703 was aspirated, and cells were incubated with Wash Buffer A twice at 37°C for 30 minutes,
704 then washed with Stellaris Wash Buffer B for 5 minutes at room temperature. Buffer was
705 aspirated and Vectashield Mounting Medium was added to the #1.5 cover glass in the
706 imaging dish and a clean coverslip was placed on top and sealed with clear nail polish.
707 Imaging dishes were stored in the dark at -20°C for up to 2 days before imaging on an
708 ONI Nanoimager S. Approximately 15 cells were imaged per genotype using the widefield
709 microscopy application. To detect smFISH probes, cells were exposed to 7% 570- or 640-

710 laser power for 1,500 milliseconds. Z-projection was obtained with 0.2 μm slices through
711 the entire cell. EGFP-FMRP was imaged sequentially which allowed us to distinguish the
712 soma and neurites from background. To analyze smFISH images, we used the FISH-
713 Quant Matlab application to detect, localize and quantify mRNA in primary motor neurons
714 (Mueller et al., 2013). Motor neuron soma and neurites were outlined individually by hand,
715 which allowed us to differentiate mRNAs residing within the soma and neurites.
716

717 **Quantification and statistical analysis**

718 All data were initially recorded in Excel (Microsoft) and then graphed and analyzed
719 in Prism version 9.0.2 (GraphPad). Results were considered statistically significant if
720 $p<0.05$. Error bars throughout the study indicate mean ± SEM. n.s. = not significant, *
721 $p<0.05$, ** $p<0.01$, *** $p<0.001$, and **** $p<0.0001$. Outliers were identified and removed
722 using ROUT method in Prism. Statistical tests and sample sizes for each experiment are
723 indicated within the corresponding figure legend and/or in methods section.
724

725 **AUTHOR CONTRIBUTIONS:**

726 Designed experiments: ELS, SAB. Performed experiments: ELS
727 Analyzed the data: ELS, SAB. Wrote the paper: ELS, SAB
728

729 **ACKNOWLEDGMENTS:**

730 We thank members of the S.A.B. lab for useful discussions. S2 cell lines and cDNAs were
731 obtained from the *Drosophila* Genomics Resource Center which is supported by NIH
732 grant 2P40OD010949. Fly lines were obtained from the Bloomington *Drosophila* Stock

733 Center which is funded by NIH grant P40OD018537. We thank Samantha Patterson for
734 assistance with FRAP experiments, Sarala Pradhan for help with developing and testing
735 the FMRP translational reporter assay, and Navneeta Kaul for assistance constructing
736 several of the *pAc5.1-FLuc 3'UTR* reporters. We are also grateful to the Knoebel Center
737 for Healthy Aging for use of the ONI NanoImager for smFISH experiments. We
738 acknowledge funding for this study to S.A.B. from NIH grant R15MH114019 and from the
739 Assistant Secretary of Defense for Health Affairs PRMRP grant W81XWH2110026.
740

741 **DECLARATION OF INTERESTS:**

742 The authors declare no competing interests.

743 **REFERENCES:**
744

745 Agulhon, C., Blanchet, P., Kobetz, A., Marchant, D., Faucon, N., Sarda, P., Moraine, C.,
746 Sittler, A., Biancalana, V., Malafosse, A., and Abitbol, M. (1999). Expression of FMR1,
747 FXR1, and FXR2 genes in human prenatal tissues. J Neuropathol Exp Neurol *58*, 867-
748 880. 10.1097/00005072-199908000-00009.

749 Antar, L.N., Afroz, R., Dictenberg, J.B., Carroll, R.C., and Bassell, G.J. (2004).
750 Metabotropic glutamate receptor activation regulates Fragile X mental retardation
751 protein and Fmr1 mRNA localization differentially in dendrites and at synapses. J
752 Neurosci *24*, 2648-2655. 10.1523/Jneurosci.0099-04.2004.

753 Antar, L.N., Dictenberg, J.B., Plociniak, M., Afroz, R., and Bassell, G.J. (2005).
754 Localization of FMRP-associated mRNA granules and requirement of microtubules for
755 activity-dependent trafficking in hippocampal neurons. Genes Brain Behav *4*, 350-359.
756 10.1111/j.1601-183X.2005.00128.x.

757 Antar, L.N., Li, C., Zhang, H., Carroll, R.C., and Bassell, G.J. (2006). Local functions for
758 FMRP in axon growth cone motility and activity-dependent regulation of filopodia and
759 spine synapses. Mol Cell Neurosci *32*, 37-48. 10.1016/j.mcn.2006.02.001.

760 Ascano, M., Jr., Mukherjee, N., Bandaru, P., Miller, J.B., Nusbaum, J.D., Corcoran,
761 D.L., Langlois, C., Munschauer, M., Dewell, S., Hafner, M., et al. (2012). FMRP targets
762 distinct mRNA sequence elements to regulate protein expression. Nature *492*, 382-386.
763 10.1038/nature11737.

764 Athar, Y.M., and Joseph, S. (2020). RNA-Binding Specificity of the Human Fragile X
765 Mental Retardation Protein. J Mol Biol *432*, 3851-3868. 10.1016/j.jmb.2020.04.021.

766 Banani, S.F., Lee, H.O., Hyman, A.A., and Rosen, M.K. (2017). Biomolecular
767 condensates: organizers of cellular biochemistry. Nat Rev Mol Cell Biol *18*, 285-298.
768 10.1038/nrm.2017.7.

769 Banani, S.F., Rice, A.M., Peeples, W.B., Lin, Y., Jain, S., Parker, R., and Rosen, M.K.
770 (2016). Compositional Control of Phase-Separated Cellular Bodies. Cell *166*, 651-663.
771 10.1016/j.cell.2016.06.010.

772 Barbee, S.A., Estes, P.S., Cziko, A.M., Hillebrand, J., Luedeman, R.A., Coller, J.M.,
773 Johnson, N., Howlett, I.C., Geng, C., Ueda, R., et al. (2006). Staufen- and FMRP-
774 containing neuronal RNPs are structurally and functionally related to somatic P bodies.
775 Neuron *52*, 997-1009. 10.1016/j.neuron.2006.10.028.

776 Basu, H., Ding, L., Pekkurnaz, G., Cronin, M., and Schwarz, T.L. (2020). Kymolyzer, a
777 Semi-Autonomous Kymography Tool to Analyze Intracellular Motility. Curr Protoc Cell
778 Biol *87*, e107. 10.1002/cpcb.107.

779 Behm-Ansmant, I., Rehwinkel, J., Doerks, T., Stark, A., Bork, P., and Izaurralde, E.
780 (2006). MRNA degradation by miRNAs and GW182 requires both CCR4 : NOT
781 deadenylase and DCP1 : DCP2 decapping complexes. Gene Dev *20*, 1885-1898.
782 10.1101/gad.1424106.

783 Bolte, S., and Cordelieres, F.P. (2006). A guided tour into subcellular colocalization
784 analysis in light microscopy. J Microsc *224*, 213-232. 10.1111/j.1365-
785 2818.2006.01706.x.

786 Chae, Y.S., Lee, S.H., Cheang, Y.H., Lee, N., Rim, Y.S., Jang, D.J., and Kaang, B.K.
787 (2010). Neuronal RNA granule contains ApCPEB1, a novel cytoplasmic polyadenylation
788 element binding protein, in Aplysia sensory neuron. Exp Mol Med *42*, 30-37.
789 10.3858/emm.2010.42.1.003.

790 Chen, E., Sharma, M.R., Shi, X., Agrawal, R.K., and Joseph, S. (2014). Fragile X
791 mental retardation protein regulates translation by binding directly to the ribosome. Mol
792 Cell *54*, 407-417. 10.1016/j.molcel.2014.03.023.

793 Cheney, P.P., Weisgerber, A.W., Feuerbach, A.M., and Knowles, M.K. (2017). Single
794 Lipid Molecule Dynamics on Supported Lipid Bilayers with Membrane Curvature.
795 Membranes (Basel) *7*. 10.3390/membranes7010015.

796 Coller, J., and Parker, R. (2005). General translational repression by activators of
797 mRNA decapping. Cell *122*, 875-886. 10.1016/j.cell.2005.07.012.

798 Cougot, N., Bhattacharyya, S.N., Tapia-Arancibia, L., Bordonne, R., Filipowicz, W.,
799 Bertrand, E., and Rage, F. (2008). Dendrites of mammalian neurons contain specialized
800 P-body-like structures that respond to neuronal activation. J Neurosci *28*, 13793-13804.
801 10.1523/JNEUROSCI.4155-08.2008.

802 Darnell, J.C., Fraser, C.E., Mostovetsky, O., and Darnell, R.B. (2009). Discrimination of
803 common and unique RNA-binding activities among Fragile X mental retardation protein
804 paralogs. Hum Mol Genet *18*, 3164-3177. 10.1093/hmg/ddp255.

805 Darnell, J.C., Fraser, C.E., Mostovetsky, O., Stefani, G., Jones, T.A., Eddy, S.R., and
806 Darnell, R.B. (2005). Kissing complex RNAs mediate interaction between the Fragile-X
807 mental retardation protein KH2 domain and brain polyribosomes. Genes Dev *19*, 903-
808 918. 10.1101/gad.1276805.

809 Darnell, J.C., Van Driesche, S.J., Zhang, C., Hung, K.Y., Mele, A., Fraser, C.E., Stone,
810 E.F., Chen, C., Fak, J.J., Chi, S.W., et al. (2011). FMRP stalls ribosomal translocation
811 on mRNAs linked to synaptic function and autism. Cell *146*, 247-261.
812 10.1016/j.cell.2011.06.013.

813 Davidovic, L., Jaglin, X.H., Lepagnol-Bestel, A.M., Tremblay, S., Simonneau, M.,
814 Bardoni, B., and Khandjian, E.W. (2007). The fragile X mental retardation protein is a
815 molecular adaptor between the neurospecific KIF3C kinesin and dendritic RNA
816 granules. Hum Mol Genet *16*, 3047-3058. 10.1093/hmg/ddm263.

817 Davis, J.K., and Broadie, K. (2017). Multifarious Functions of the Fragile X Mental
818 Retardation Protein. Trends Genet *33*, 703-714. 10.1016/j.tig.2017.07.008.

819 De Boulle, K., Verkerk, A.J., Reyniers, E., Vits, L., Hendrickx, J., Van Roy, B., Van den
820 Bos, F., de Graaff, E., Oostra, B.A., and Willems, P.J. (1993). A point mutation in the

821 FMR-1 gene associated with fragile X mental retardation. Nat Genet *3*, 31-35.
822 10.1038/ng0193-31.

823 Dictenberg, J.B., Swanger, S.A., Antar, L.N., Singer, R.H., and Bassell, G.J. (2008). A
824 direct role for FMRP in activity-dependent dendritic mRNA transport links filopodial-
825 spine morphogenesis to fragile X syndrome. Dev Cell *14*, 926-939.
826 10.1016/j.devcel.2008.04.003.

827 Drozd, M., Bardoni, B., and Capovilla, M. (2018). Modeling Fragile X Syndrome in
828 Drosophila. Front Mol Neurosci *11*, 124. 10.3389/fnmol.2018.00124.

829 El Fatimy, R., Davidovic, L., Tremblay, S., Jaglin, X., Dury, A., Robert, C., De Koninck,
830 P., and Khandjian, E.W. (2016). Tracking the Fragile X Mental Retardation Protein in a
831 Highly Ordered Neuronal RiboNucleoParticles Population: A Link between Stalled
832 Polyribosomes and RNA Granules. Plos Genet *12*, e1006192.
833 10.1371/journal.pgen.1006192.

834 Estes, P.S., O'Shea, M., Clasen, S., and Zarnescu, D.C. (2008). Fragile X protein
835 controls the efficacy of mRNA transport in Drosophila neurons. Mol Cell Neurosci *39*,
836 170-179. 10.1016/j.mcn.2008.06.012.

837 Feng, Y., Absher, D., Eberhart, D.E., Brown, V., Malter, H.E., and Warren, S.T. (1997).
838 FMRP associates with polyribosomes as an mRNP, and the I304N mutation of severe

839 fragile X syndrome abolishes this association. Mol Cell *1*, 109-118. 10.1016/s1097-
840 2765(00)80012-x.

841 Formicola, N., Vijayakumar, J., and Besse, F. (2019). Neuronal ribonucleoprotein
842 granules: Dynamic sensors of localized signals. Traffic *20*, 639-649. 10.1111/tra.12672.

843 Gareau, C., Houssin, E., Martel, D., Coudert, L., Mellaoui, S., Huot, M.E., Laprise, P.,
844 and Mazroui, R. (2013a). Characterization of fragile X mental retardation protein
845 recruitment and dynamics in Drosophila stress granules. PLoS One *8*, e55342.
846 10.1371/journal.pone.0055342.

847 Gareau, C., Martel, D., Coudert, L., Mellaoui, S., and Mazroui, R. (2013b).
848 Characterization of Fragile X Mental Retardation Protein granules formation and
849 dynamics in Drosophila. Biol Open *2*, 68-81. 10.1242/bio.20123012.

850 Goering, R., Hudish, L.I., Guzman, B.B., Raj, N., Bassell, G.J., Russ, H.A., Dominguez,
851 D., and Taliaferro, J.M. (2020). FMRP promotes RNA localization to neuronal
852 projections through interactions between its RGG domain and G-quadruplex RNA
853 sequences. Elife *9*. ARTN e52621
854 10.7554/eLife.52621.

855 Gopal, P.P., Nirschl, J.J., Klinman, E., and Holzbaur, E.L. (2017). Amyotrophic lateral
856 sclerosis-linked mutations increase the viscosity of liquid-like TDP-43 RNP granules in
857 neurons. Proc Natl Acad Sci U S A *114*, E2466-E2475. 10.1073/pnas.1614462114.

858 Ishizuka, A., Siomi, M.C., and Siomi, H. (2002). A Drosophila fragile X protein interacts
859 with components of RNAi and ribosomal proteins. Gene Dev *16*, 2497-2508.
860 10.1101/gad.1022002.

861 Kim, S.H., Dong, W.K., Weiler, I.J., and Greenough, W.T. (2006). Fragile X mental
862 retardation protein shifts between polyribosomes and stress granules after neuronal
863 injury by arsenite stress or in vivo hippocampal electrode insertion. J Neurosci *26*, 2413-
864 2418. 10.1523/Jneurosci.3680-05.2006.

865 Kim, T.H., Tsang, B., Vernon, R.M., Sonenberg, N., Kay, L.E., and Forman-Kay, J.D.
866 (2019). Phospho-dependent phase separation of FMRP and CAPRIN1 recapitulates
867 regulation of translation and deadenylation. Science *365*, 825-829.
868 10.1126/science.aax4240.

869 Kroschwald, S., Maharana, S., and Alberti, S. (2017). Hexanediol: a chemical probe to
870 investigate the material properties of membrane-less compartments. Matters.
871 10.19185/matters.201702000010.

872 Lai, A., Valdez-Sinon, A.N., and Bassell, G.J. (2020). Regulation of RNA granules by
873 FMRP and implications for neurological diseases. Traffic *21*, 454-462.
874 10.1111/tra.12733.

875 Li, C., Bassell, G.J., and Sasaki, Y. (2009). Fragile X Mental Retardation Protein is
876 Involved in Protein Synthesis-Dependent Collapse of Growth Cones Induced by
877 Semaphorin-3A. Front Neural Circuits *3*, 11. 10.3389/neuro.04.011.2009.

878 Li, P., Banjade, S., Cheng, H.C., Kim, S., Chen, B., Guo, L., Llaguno, M., Hollingsworth,
879 J.V., King, D.S., Banani, S.F., et al. (2012). Phase transitions in the assembly of
880 multivalent signalling proteins. Nature *483*, 336-340. 10.1038/nature10879.

881 Mittag, T., and Parker, R. (2018). Multiple Modes of Protein-Protein Interactions
882 Promote RNP Granule Assembly. J Mol Biol *430*, 4636-4649.
883 10.1016/j.jmb.2018.08.005.

884 Molliex, A., Temirov, J., Lee, J., Coughlin, M., Kanagaraj, A.P., Kim, H.J., Mittag, T., and
885 Taylor, J.P. (2015). Phase separation by low complexity domains promotes stress
886 granule assembly and drives pathological fibrillization. Cell *163*, 123-133.
887 10.1016/j.cell.2015.09.015.

888 Morales, J., Hiesinger, P.R., Schroeder, A.J., Kume, K., Verstreken, P., Jackson, F.R.,
889 Nelson, D.L., and Hassan, B.A. (2002). Drosophila fragile X protein, DFXR, regulates
890 neuronal morphology and function in the brain. Neuron *34*, 961-972. Doi
891 10.1016/S0896-6273(02)00731-6.

892 Mueller, F., Senecal, A., Tantale, K., Marie-Nelly, H., Ly, N., Collin, O., Basyuk, E.,
893 Bertrand, E., Darzacq, X., and Zimmer, C. (2013). FISH-quant: automatic counting of
894 transcripts in 3D FISH images. Nat Methods *10*, 277-278. 10.1038/nmeth.2406.

895 Myrick, L.K., Deng, P.Y., Hashimoto, H., Oh, Y.M., Cho, Y., Poidevin, M.J., Suhl, J.A.,
896 Visootsak, J., Cavalli, V., Jin, P., et al. (2015a). Independent role for presynaptic FMRP
897 revealed by an FMR1 missense mutation associated with intellectual disability and
898 seizures. Proc Natl Acad Sci U S A *112*, 949-956. 10.1073/pnas.1423094112.

899 Myrick, L.K., Hashimoto, H., Cheng, X., and Warren, S.T. (2015b). Human FMRP
900 contains an integral tandem Agenet (Tudor) and KH motif in the amino terminal domain.
901 Hum Mol Genet *24*, 1733-1740. 10.1093/hmg/ddu586.

902 Myrick, L.K., Nakamoto-Kinoshita, M., Lindor, N.M., Kirmani, S., Cheng, X., and Warren,
903 S.T. (2014). Fragile X syndrome due to a missense mutation. Eur J Hum Genet *22*,
904 1185-1189. 10.1038/ejhg.2013.311.

905 Nesler, K.R., Sand, R.I., Symmes, B.A., Pradhan, S.J., Boin, N.G., Laun, A.E., and
906 Barbee, S.A. (2013). The miRNA pathway controls rapid changes in activity-dependent
907 synaptic structure at the Drosophila melanogaster neuromuscular junction. PLoS One *8*,
908 e68385. 10.1371/journal.pone.0068385.

909 Patel, A., Lee, H.O., Jawerth, L., Maharana, S., Jahnel, M., Hein, M.Y., Stoynov, S.,
910 Mahamid, J., Saha, S., Franzmann, T.M., et al. (2015). A Liquid-to-Solid Phase

911 Transition of the ALS Protein FUS Accelerated by Disease Mutation. Cell *162*, 1066-
912 1077. 10.1016/j.cell.2015.07.047.

913 Pieretti, M., Zhang, F.P., Fu, Y.H., Warren, S.T., Oostra, B.A., Caskey, C.T., and
914 Nelson, D.L. (1991). Absence of expression of the FMR-1 gene in fragile X syndrome.
915 Cell *66*, 817-822. 10.1016/0092-8674(91)90125-i.

916 Pradhan, S.J., Nesler, K.R., Rosen, S.F., Kato, Y., Nakamura, A., Ramaswami, M., and
917 Barbee, S.A. (2012). The conserved P body component HPat/Pat1 negatively regulates
918 synaptic terminal growth at the larval Drosophila neuromuscular junction. J Cell Sci *125*,
919 6105-6116. 10.1242/jcs.113043.

920 Prieto, M., Folci, A., Poupon, G., Schiavi, S., Buzzelli, V., Pronot, M., Francois, U.,
921 Pousinha, P., Lattuada, N., Abelanet, S., et al. (2021). Missense mutation of Fmr1
922 results in impaired AMPAR-mediated plasticity and socio-cognitive deficits in mice. Nat
923 Commun *12*, 1557. 10.1038/s41467-021-21820-1.

924 Ray, D., Kazan, H., Cook, K.B., Weirauch, M.T., Najafabadi, H.S., Li, X., Gueroussov,
925 S., Albu, M., Zheng, H., Yang, A., et al. (2013). A compendium of RNA-binding motifs
926 for decoding gene regulation. Nature *499*, 172-177. 10.1038/nature12311.

927 Reeve, S.P., Bassetto, L., Genova, G.K., Kleyner, Y., Leyssen, M., Jackson, F.R., and
928 Hassan, B.A. (2005). The Drosophila fragile X mental retardation protein controls actin

929 dynamics by directly regulating profilin in the brain. Curr Biol *15*, 1156-1163.
930 10.1016/j.cub.2005.05.050.

931 Richter, J.D., and Zhao, X. (2021). The molecular biology of FMRP: new insights into
932 fragile X syndrome. Nat Rev Neurosci. 10.1038/s41583-021-00432-0.

933 Santoro, M.R., Bray, S.M., and Warren, S.T. (2012). Molecular mechanisms of fragile X
934 syndrome: a twenty-year perspective. Annu Rev Pathol *7*, 219-245. 10.1146/annurev-
935 pathol-011811-132457.

936 Schwartz, J.C., Wang, X., Podell, E.R., and Cech, T.R. (2013). RNA seeds higher-order
937 assembly of FUS protein. Cell Rep *5*, 918-925. 10.1016/j.celrep.2013.11.017.

938 Shin, Y., and Brangwynne, C.P. (2017). Liquid phase condensation in cell physiology
939 and disease. Science *357*. 10.1126/science.aaf4382.

940 Sudhakaran, I.P., Hillebrand, J., Dervan, A., Das, S., Holohan, E.E., Hulsmeier, J.,
941 Sarov, M., Parker, R., VijayRaghavan, K., and Ramaswami, M. (2014). FMRP and
942 Ataxin-2 function together in long-term olfactory habituation and neuronal translational
943 control. Proc Natl Acad Sci U S A *111*, E99-E108. 10.1073/pnas.1309543111.

944 Suhl, J.A., Chopra, P., Anderson, B.R., Bassell, G.J., and Warren, S.T. (2014). Analysis
945 of FMRP mRNA target datasets reveals highly associated mRNAs mediated by G-

946 quadruplex structures formed via clustered WGGA sequences. Hum Mol Genet *23*,
947 5479-5491. 10.1093/hmg/ddu272.

948 Suhl, J.A., and Warren, S.T. (2015). Single-Nucleotide Mutations in FMR1 Reveal Novel
949 Functions and Regulatory Mechanisms of the Fragile X Syndrome Protein FMRP. J Exp
950 Neurosci *9*, 35-41. 10.4137/JEN.S25524.

951 Tourriere, H., Chebli, K., Zekri, L., Courselaud, B., Blanchard, J.M., Bertrand, E., and
952 Tazi, J. (2003). The RasGAP-associated endoribonuclease G3BP assembles stress
953 granules. J Cell Biol *160*, 823-831. 10.1083/jcb.200212128.

954 Tsang, B., Arsenault, J., Vernon, R.M., Lin, H., Sonenberg, N., Wang, L.Y., Bah, A., and
955 Forman-Kay, J.D. (2019). Phosphoregulated FMRP phase separation models activity-
956 dependent translation through bidirectional control of mRNA granule formation. Proc
957 Natl Acad Sci U S A *116*, 4218-4227. 10.1073/pnas.1814385116.

958 Valverde, R., Pozdnyakova, I., Kajander, T., Venkatraman, J., and Regan, L. (2007).
959 Fragile X mental retardation syndrome: structure of the KH1-KH2 domains of fragile X
960 mental retardation protein. Structure *15*, 1090-1098. 10.1016/j.str.2007.06.022.

961 Van Treeck, B., and Parker, R. (2018). Emerging Roles for Intermolecular RNA-RNA
962 Interactions in RNP Assemblies. Cell *174*, 791-802. 10.1016/j.cell.2018.07.023.

963 Vijayakumar, J., Perrois, C., Heim, M., Bousset, L., Alberti, S., and Besse, F. (2019).
964 The prion-like domain of Drosophila Imp promotes axonal transport of RNP granules in
965 vivo. Nat Commun *10*, 2593. 10.1038/s41467-019-10554-w.

966 Wan, L., Dockendorff, T.C., Jongens, T.A., and Dreyfuss, G. (2000). Characterization of
967 dFMR1, a Drosophila melanogaster homolog of the fragile X mental retardation protein.
968 Mol Cell Biol *20*, 8536-8547. 10.1128/mcb.20.22.8536-8547.2000.

969 Xu, K., Bogert, B.A., Li, W., Su, K., Lee, A., and Gao, F.B. (2004). The fragile X-related
970 gene affects the crawling behavior of Drosophila larvae by regulating the mRNA level of
971 the DEG/ENaC protein pickpocket1. Curr Biol *14*, 1025-1034.
972 10.1016/j.cub.2004.05.055.

973 Zang, J.B., Nosyreva, E.D., Spencer, C.M., Volk, L.J., Musunuru, K., Zhong, R., Stone,
974 E.F., Yuva-Paylor, L.A., Huber, K.M., Paylor, R., et al. (2009). A mouse model of the
975 human Fragile X syndrome I304N mutation. Plos Genet *5*, e1000758.
976 10.1371/journal.pgen.1000758.

977 Zhang, Y., O'Connor, J.P., Siomi, M.C., Srinivasan, S., Dutra, A., Nussbaum, R.L., and
978 Dreyfuss, G. (1995). The fragile X mental retardation syndrome protein interacts with
979 novel homologs FXR1 and FXR2. Embo J *14*, 5358-5366.

980 Zhang, Y.Q., Bailey, A.M., Matthies, H.J., Renden, R.B., Smith, M.A., Speese, S.D.,
981 Rubin, G.M., and Broadie, K. (2001). Drosophila fragile X-related gene regulates the

982 MAP1B homolog Futsch to control synaptic structure and function. Cell *107*, 591-603.

983 10.1016/s0092-8674(01)00589-x.

984